

CONFERENCES AND SYMPOSIA

PACS number: 01.10.Fv

Scientific session of the Physical Sciences Division of the Russian Academy of Sciences (12 April 2006)

A scientific session of the Physical Sciences Division of the Russian Academy of Sciences was held in the Conference Hall of the Lebedev Physics Institute, Russian Academy of Sciences, on 12 April 2006. The following reports were presented at the session:

(1) **Khokhlov D R** (Lomonosov Moscow State University) "High-sensitivity terahertz radiation detectors based on a new class of semiconductor materials";

(2) **Mitin A V** (Kazan State Technological University) "Modulation gamma-resonance spectroscopy";

(3) **Kurochkin V E** (Institute of Analytical Instrumentation, Russian Academy of Sciences, St. Petersburg) "Methods and tools for the express immunoassay. A new approach to solving the problem";

(4) **Lukin V P** (Institute of Atmospheric Optics, Siberian Division of the Russian Academy of Sciences, Tomsk) "Adaptive optical imaging in the atmosphere."

A brief presentation of the reports is given below.

PACS numbers: **07.57.–c**, **78.20.–e**, **85.30.–z**
DOI: 10.1070/PU2006v049n09ABEH006094

High-sensitivity terahertz radiation detectors based on a new class of semiconductor materials

D R Khokhlov

1. Introduction

Modern trends in the development of physics in the area of optoelectronics are moving towards an increase in the operating wavelength of the corresponding devices to several dozen or hundred micrometers. The terahertz range of electromagnetic waves occupies a special place among the existing problems. This is precisely the spectral range that corresponds to the characteristic phonon frequencies in solids and the rotational–vibrational modes of heavy molecules, which is of great interest to spectroscopic research. Furthermore, many important problems in entirely different fields of science are related to the investigation of terahertz radiation, e.g., in space research and biomedicine. Among the rapidly advancing areas of the practical application of terahertz spectroscopy is remote selective probing of dielectric objects. These include many organic materials and, in particular, explosives.

Uspekhi Fizicheskikh Nauk **176** (9) 983 – 1006 (2006)
Translated by E N Ragozin, E Yankovsky, Yu V Morozov; edited by A M Semikhatov

Progress in this area is moderated by the fact that both radiophysical techniques — on the longer wavelength side — and optical ones — on the shorter wavelength side — operate poorly in the terahertz range. In particular, the sensitivity of terahertz radiation detectors is substantially lower than the sensitivity of infrared and radio-frequency radiation detectors.

The majority of high-sensitivity photodetection systems operating in the terahertz electromagnetic wave range have been traditionally made on the basis of lightly doped germanium or silicon. The longest photoelectric threshold wavelength (~ 220 μm) corresponds to uniaxially strained Ge(Ga) [1]. The most important advantage of germanium and silicon is the extremely well-proven technology of crystal growth, which enables producing materials with a very low uncontrollable impurity density. At the same time, external action, like hard radiation, may introduce a large number of defects in an initially extremely pure or perfect material, which degrades the performance of the corresponding photodetection devices.

This report is concerned with the opportunities furnished by the use of alternative materials — doped alloys based on lead tellurides — for recording low-intensity terahertz radiation.

2. Basic properties of doped alloys based on lead telluride

Lead chalcogenides are widely used in infrared optoelectronics, primarily in the fabrication of lasers and light-emitting diodes operating in the medium- and far-infrared (IR) ranges [2]. Furthermore, considerable progress has been reached in the production of photodiode arrays with a large number of elements, which are sputtered on silicon substrates via fluoride buffer layers [3]. The use of alloys on the basis of lead telluride doped with elements of group III opens up new interesting possibilities due to the emergence of qualitatively new physical properties in the doped material. The specific properties inherent in lead telluride-based alloys may provide improvement in the performance of the corresponding photodetector devices in comparison with the existing analogues.

2.1 Fermi-level stabilization

Lead telluride-based alloys are ternary or quadruple solid solutions of the IV–VI group semiconductors heavily doped with some impurities (which typically belong to group III): $Pb_{1-x}Sn_xTe$(In), $Pb_{1-x}Mn_xTe$(In), $Pb_{1-x}Mn_xTe$(Ga), PbTe(Ga), $Pb_{1-x-y}Sn_xGe_yTe$(In), $Pb_{1-x}Ge_xTe$(Ga,Yb), etc. (see the comprehensive review in Ref. [4]). This doping leads to the formation of deep local or quasilocal levels in the semiconductor spectrum. When an impurity is introduced in quantities exceeding the density of other electrically active

impurities and defects, the position of the Fermi level is stabilized by these deep levels, i.e., remains invariable under additional doping by other impurities. This results in a high degree of uniformity of electrophysical crystal properties and the temporal stability of their characteristics. In particular, the energy fluctuations ΔE_c of the bottom of the conduction band do not exceed ~ 0.1 meV for the Fermi energy ~ 100 meV above the bottom of the conduction band. These fluctuations are substantially smaller than even the fluctuations in undoped alloys or in other narrow-gap semiconductor alloys like $Hg_{1-x}Cd_xTe$, in which the fluctuations in the width of the forbidden band are normally equal to about 20 meV.

The Fermi level can be stabilized in both the allowed bands and the forbidden gap, depending on the alloy composition. Therefore, varying the alloy composition allows changing the properties of the system from 'dielectric' to 'metallic' ones. There is a possibility to vary the dark conductivity over very wide limits (from $\rho \sim 10^{-2}\ \Omega$ cm to $\rho \sim 10^{9}\ \Omega$ cm) with retention of high charge carrier mobility ($\mu \sim 10^5\ \text{cm}^2\,\text{V}^{-1}\,\text{s}^{-1}$). The dark density of electrons or holes may vary between $10^{18}\ \text{cm}^{-3}$ and $n, p < 10^9\ \text{cm}^{-3}$. The low values of n and p are realized in the semi-insulating state of alloys, when the Fermi level is stabilized inside the forbidden band. Because the impurity states that furnish the Fermi level stabilization are deep, the hydrogen-like states of impurity centers are not formed. That is why the dark currents in lead telluride-based alloys are substantially lower than in impurity photodetectors on the basis of Ge or Si for the same wavelength and temperature.

Therefore, the doping entails a highly unusual situation, whereby a heavily doped narrow-gap semiconductor with a large number of growth defects behaves as a virtually perfect semiconductor with a zero background density of charge carriers and a very high uniformity of electrophysical parameters. Such an 'internal purification' of the material underlies its relative cheapness in production and makes the idea of using these materials as IR detectors extremely attractive.

2.2 Persistent photoconductivity

A radically new feature of lead telluride-based alloys responsible for the occurrence of a high photoresponse is the existence of a barrier W between the impurity and band states in the energy spectrum. The existence of this barrier results in long lifetimes, $\tau \sim 10^5$ s, of nonequilibrium electrons. For the temperature $T < 20$ K (for $Pb_{1-x}Sn_xTe$(In)-type alloys) or $T < 80$ K (for PbTe(Ga)-type alloys), the material is actually a photodetector with an internal signal integration, which eliminates the necessity of using complex external integrating circuits. Moreover, the Maxwellian relaxation time shortens in internal integration with time, which determines a faster response. Lead telluride-based alloys are also capable of operating as conventional photodetectors without internal signal integration in the temperature region $T \sim T_c$. The characteristic lifetime of nonequilibrium charge carriers may be varied over a wide range (from 10^{-4} to 10^5 s) for $T = 4.2$ K by changing the alloy composition, in addition to the possibility of controlling this parameter by changing the semiconductor temperature.

Internal signal integration emerges because the characteristic lifetime of a photoexcited free electron is much longer than the characteristic measurement time. In this situation, lengthening the exposure time leads to a linear increase in the photoresponse because the excited electrons can hardly recombine.

2.3 Theoretical models

Several models have been proposed to account for the occurrence of slow relaxation processes in lead telluride-based alloys.

Kagan and Kikoin [5] proposed a model to account for the occurrence of slow relaxation processes at low temperatures. In the framework of the concepts described in Ref. [5], the long lifetimes of nonequilibrium charge carriers at low temperatures are related to the autolocalization barrier emerging in the change of impurity charge state. In the ionization of an impurity center, configuration restructuring of the local crystal environment of the impurity atom occurs. In this case, in order to recombine, an electron has to overcome the barrier in the configuration space associated with the need to polarize the crystal lattice in the vicinity of the impurity center in localization of the nonequilibrium electron. The authors of several subsequent papers [6–8] proposed different mechanisms of this polarization, which, however, basically differed little from each other.

It was shown in Refs [9–12] that the observed data cannot be explained in the framework of the model taking the existence of only one local state into account. In particular, this manifests itself in the photoresponse kinetics, upon turning out the illumination, exhibiting two portions — a fast ($\sim 1-10$ ms) and slow (10 ms – 10^4 s, depending on the temperature) relaxation of conductivity. To describe this and several other results, the model in Ref. [5] was substantially augmented [9]. According to Zasavitskii et al. [9], apart from the ground impurity state, which furnishes stabilization of the Fermi level and is a two-electron state, there is also a metastable one-electron impurity state. The latter state is separated by a barrier in the configuration space both from the ground two-electron local state and from the state with delocalized charge carriers in the allowed band. In this case, the localization of photoexcited charge carriers proceeds in two stages — fast and slow relaxation. The fast photoconductivity relaxation corresponds to recombination to the metastable local state, and the slow relaxation portion corresponds to recombination to the ground impurity state.

Belogorokhov et al. [13] proposed a somewhat different concept. The model in Ref. [13] relies on the fact that the actual bands in lead chalcogenides are built almost entirely of atomic p-orbitals. A group-III impurity atom replaces a lead atom in the doping of the above materials. The effect of Fermi level stabilization arises from the fact that the charge state of the impurity atom Im^{2+}, which is neutral relative to the crystal lattice, is unstable and decays according to the reaction $2Im^{2+} \rightarrow Im^{+} + Im^{3+}$.

In terms of atomic orbitals, the Im^{2+} state corresponds to the s^1p^2 electron configuration, the Im^{+} state corresponds to the s^2p^1 configuration, and the Im^{3+} state to the s^0p^3 configuration. The s^2p^2 configuration corresponds to the lead atom replaced by the impurity. The allowed bands in lead chalcogenides are almost entirely built of atomic p-orbitals, and therefore the electrons residing in the deep s-shell are localized for different charge states of the impurity atom, while p-electrons are delocalized.

The main idea of the model in Ref. [13] consists in the one-electron impurity state, in which only one electron is in the s-state, located (in the one-electron approximation) much higher in energy than the ground two-electron state and

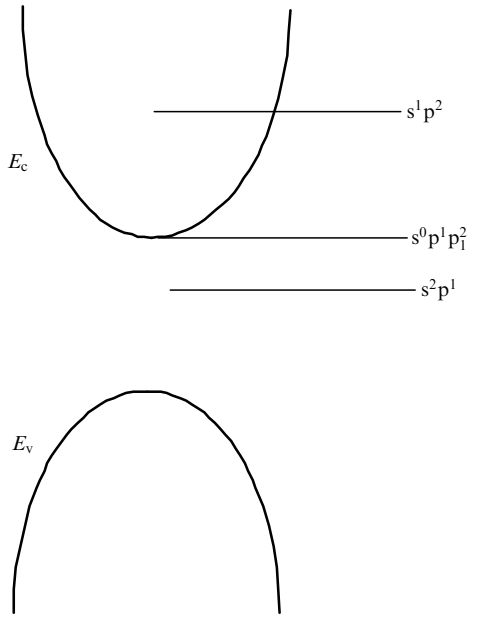

Figure 1. Model of the energy spectrum of an impurity center [13]; E_c corresponds to the edge of the conduction band; E_v is the edge of the valence band.

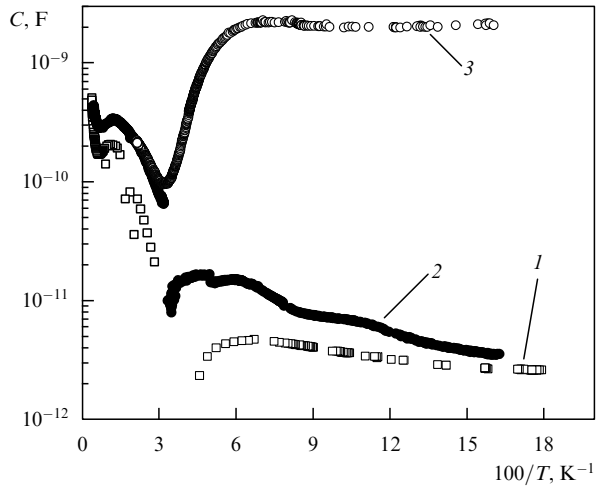

Figure 2. Temperature dependences of the capacitance C for a $Pb_{0.75}Sn_{0.25}Te(In)$ sample obtained at the frequencies 1 MHz (1) and 50 kHz (*2*, *3*). Curves *1* and *2* were measured under dark screening conditions, curve *3* was obtained under illumination by a thermal radiation source [17].

above the bottom of the conduction band (Fig. 1). Then, in the photoionization of the first electron from the impurity center, an energy sufficient, first, to transfer this electron to the conduction band and, second, to transfer the impurity center to the state corresponding to one s-electron localized on the impurity needs to be imparted. The single s-electron remaining at the impurity center rapidly transits to the conduction band, whose bottom lies lower in energy. Therefore, two nonequilibrium electrons emerge in the conduction band. Recombination is a one-electron process, but for the impurity center to capture an electron, the electron should be imparted an energy equal to the difference between the energies of the Fermi quasilevel and the one-electron impurity state. This energy gap is in fact the energy barrier that impedes fast electron recombination at the center.

However, the reasons why two portions of photoconductivity relaxation emerge remain unclear in the framework of the above model. A possible resolution of this contradiction is as follows. Stabilization of the Fermi level implies that a significant number of gallium atoms have an empty s-shell. Two p-electrons with oppositely directed spins may be localized in the attractive potential of this shell [14]. However, it may be that a single impurity center with an empty s-shell is unable to produce a bound state because of the large permittivity value and the low effective electron mass in PbTe. At the same time, the number of such centers is quite large, and one bound p-electron state may be formed with the simultaneous participation of a large number (up to $10^4 - 10^5$) of impurity centers having an empty s-shell [15]. Then, the fast photoconductivity relaxation may be caused by the localization of a part of the photoexcited electrons in these bound states, which are located in energy near the bottom of the conduction band and are shallow in this sense.

An estimate of the localization radius for this state yields a huge value, of the order of 100 nm. The filling of these states may occur either at low temperatures under photoexcitation or at a higher temperature in darkness. Because the electron localization radius is long, the filling of metastable states is expected to entail a giant dielectric response. This effect is indeed observed [16, 17]: the effective material permittivity increases by more than two orders of magnitude on raising the temperature and under infrared illumination (Fig. 2).

2.4 Spectral characteristics

The characteristic energy values in the spectrum, which can be varied by changing the material composition, determine a high photosensitivity of the materials in a wide wavelength range (from 1 μm to several hundred micrometers). The characteristic energies of the semiconductor spectrum and, accordingly, the threshold photoresponse values are determined by the alloy composition.

Kristovskii et al. [18] reported the discovery of a photoresponse in a $Pb_{0.75}Sn_{0.25}Te(In)$ film at the wavelengths 176 and 241 μm. The $Pb_{0.75}Sn_{0.25}Te(In)$ film was grown by molecular-beam epitaxy on a BaF_2 substrate. The thermal activation energy of the ground impurity state was calculated from the relation $\rho \sim \exp(E_a/2kT)$ and was equal to 20 meV. The experiment was carried out at a facility with complete screening of background radiation. A blackbody with the temperature 77 K or 300 K was the source of infrared radiation. Several cooled filters formed the narrow spectral band of radiation directed onto the sample. The temporal kinetics of the current flowing through the sample was recorded under different voltages across the sample and different blackbody temperatures. The experimental data obtained for the voltage 10 mV and the blackbody temperature 300 K are depicted in Fig. 3.

Appreciable photoresponse was recorded for both wavelengths of radiation incident on the sample. We note several features of the photoconduction. First of all, the temporal current buildup kinetics is strongly nonlinear. Removing the illumination results in a fast photocurrent decay with a subsequent slow relaxation to the dark value. However, turning on the illumination shortly after its removal has the effect that the photocurrent rapidly, in a time comparable to the 'fast' relaxation time, builds up to the value that existed prior to the removal of illumination, with the subsequent

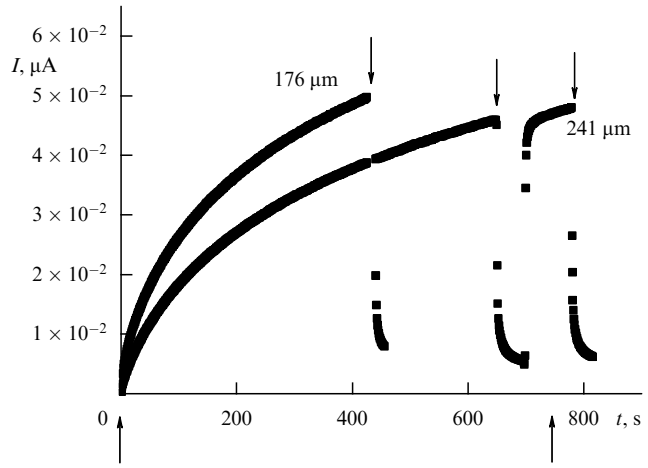

Figure 3. Photocurrent buildup and decline kinetics for the voltage 10 mV across the sample and different wavelengths of exciting radiation, which are indicated in the figure. Arrows indicate the moments at which infrared illumination was engaged and turned off [18].

resumption of the previous, relatively slow, dynamics of photocurrent buildup. Clearly, the fast and slow relaxation processes are essentially different in nature.

The second significant point is as follows. The photon energy corresponding to radiation wavelengths 176 and 241 μm is substantially lower than the thermal activation energy of the ground impurity state. Therefore, the results in Ref. [18] are direct evidence that the persistent photoconductivity in $Pb_{1-x}Sn_xTe(In)$ may be caused by the photoexcitation of metastable impurity states. The threshold energy for the optical excitation of these states is very low. The wavelength of the corresponding photon is longer than 241 μm, which is the greatest value for the photoelectric threshold in nonthermal radiation detectors. The photosensitivity cutoff for the materials under consideration is supposedly in a substantially longer wavelength region. It is not unlikely that the working range of $Pb_{1-x}Sn_xTe(In)$-based photodetectors spans the entire terahertz range. On the other hand, the nature of the emergence of two portions of free-electron generation and recombination remains unclear in this case, because the ground impurity state should be 'excluded from play' because the exciting photon energy is low.

2.5 Radiometric characteristics

Internal signal integration is an advantage only when a possibility to nullify the stored photosignal exists. We have developed an efficient technique of quenching the persistent photoconductivity in lead telluride-based alloys. Microwave pulses (200 – 400 MHz) applied to the sample were found to completely quench the persistent photoconductivity (PC) in $10^{-5}-10^{-6}$ s [19]. This signifies that the possibility exists of implementing the regime of periodic storage of a photosignal followed by its fast nullification.

Furthermore, under a certain regime of quenching of the residual PC by microwave pulses, the quantum efficiency of the material increases to ~ 100 upon exposure to the quenching pulse [19], i.e., every incident photon produces at least 100 free electrons in the conduction band. This effect is related to the specific character of impurity states. It furnishes a high current responsivity (10^9 A^2 W^{-1}), which was recorded for a single photodetector based on $Pb_{0.75}Sn_{0.25}Te(In)$ operating in the above regime with the readout frequency 10 Hz. In this test, it has been possible to record the radiation power 10^{16} W at the wavelength 18 μm (determined by a mesh filter), even though the measuring technique in use did not enable measuring a current below 10^{-7} A. The above parameters correspond to recording about 10^3 photons per 1 cm^2 in 1 s [20].

2.6 'Continuous' focal-plane array

It was established that local illumination of a part of a photodetector sample results in a local excitation of nonequilibrium charge carriers, which do not diffuse into the unilluminated domains at low temperatures. Therefore, there is a one-to-one correspondence between the radiation intensity distribution over the sample surface and the distribution of the nonequilibrium charge carrier density [21]. In other words, the alloys under consideration allow making photodetector arrays in which each effective element effects internal signal accumulation. The dimension of the shaded interval between the elements of the array required to eliminate their interference is theoretically estimated at about 10 μm. This is the characteristic dimension corresponding to the spatial distribution of the free charge carriers at the edge of a 'light spot.' Our experiments have shown that this characteristic dimension is below 200 μm. The geometric noise in arrays of this type is minimized due to the high degree of spatial uniformity of the electrophysical material parameters. The idea of a simple technique for information readout from such an array has been elaborated, which so far has not been realized because of technical problems.

2.7 Radiation hardness

The position of the Fermi level in crystals depends neither on the impurity density fluctuations nor on the fluctuations of intrinsic lattice defects, including radiation-induced ones, over a wide range. The possibility of dividing the impurity states into states with different charges underlies the high radiation hardness of the parameters of lead telluride-based alloys, which is at least four orders of magnitude higher than in the known analogues (with the exception of blocked-impurity-band structures). Exposure of the alloys to fast 6 MeV electrons in an accelerator showed that the photoconduction parameters in $Pb_{1-x}Sn_xTe(In)$ and PbTe(Ga) (with the In, Ga content $\sim 0.2-0.4$ at. %) remained invariable (to within $\sim 5\%$) under electron fluxes Φ up to 10^{18} cm^{-2} [22].

3. Conclusions

Thus, a unique combination of physical properties makes lead telluride-based alloys highly attractive for constructing extremely sensitive focal-plane arrays for the photodetection of terahertz radiation. The $Pb_{1-x}Sn_xTe(In)$ photodetectors exhibit the following distinguishing features that permit them to successfully compete with the existing analogues:

- internal integration of the incident light flux;
- the possibility of efficient and rapid quenching of the accumulated signal;
- microwave stimulation of quantum efficiency up to 10^2;
- the feasibility of realizing a 'continuous' focal-plane array;
- the possibility of realizing a simple readout method;
- a high radiation hardness.

This work was supported in part by the Russian Foundation for Basic Research (Grant Nos 04-02-16497,

05-02-16657, 06-02-90867) and the Swiss National Science Foundation (Grant No. IB7320-110921/1).

References

1. Haller E E, Hueschen M R, Richards P L *Appl. Phys. Lett.* **34** 495 (1979)
2. Lambrecht A et al. *Semicond. Sci. Technol.* **8** S334 (1993)
3. Zogg H et al. *Semicond. Sci. Technol.* **6** C36 (1991)
4. Volkov B A, Ryabova L I, Khokhlov D R *Usp. Fiz. Nauk* **172** 875 (2002) [*Phys. Usp.* **45** 819 (2002)]
5. Kagan Yu, Kikoin K A *Pis'ma Zh. Eksp. Teor. Fiz.* **31** 367 (1980) [*JETP Lett.* **31** 335 (1980)]
6. Litvinov V I, Tovstyuk K D *Fiz. Tverd. Tela* **24** 896 (1982)
7. Pankratov O A, Volkov B A *Zh. Eksp. Teor. Fiz.* **88** 280 (1985) [*Sov. Phys. JETP* **61** 164 (1985)]
8. Pankratov O A, Volkov B A *Sov. Sci. Reviews Sect. A: Phys.* (Ed. I M Khalatnikov) **9** 355 (1987)
9. Zasavitskii I I et al. *Pis'ma Zh. Eksp. Teor. Fiz.* **42** 3 (1985) [*JETP Lett.* **42** 1 (1985)]
10. Zasavitskii I I et al. *Fiz. Tekh. Poluprovodn.* **20** 214 (1986)
11. Vinchakov V N et al. *Pis'ma Zh. Eksp. Teor. Fiz.* **43** 384 (1986) [*JETP Lett.* **43** 495 (1986)]
12. Akimov B A et al. *Fiz. Tekh. Poluprovodn.* **23** 668 (1989) [*Sov. Phys. Semicond.* **23** 418 (1989)]
13. Belogorokhov A I et al. *Pis'ma Zh. Eksp. Teor. Fiz.* **72** 178 (2000) [*JETP Lett.* **72** 123 (2000)]
14. Volkov B A, Ruchaiskii O M *Pis'ma Zh. Eksp. Teor. Fiz.* **62** 205 (1995) [*JETP Lett.* **62** 217 (1995)]
15. Baz' A I, Zel'dovich Ya B, Perelomov A M *Rasseyanie, Reaktsii i Raspady v Nerelyativistskoi Kvantovoi Mekhanike* 2nd ed. (Moscow: Nauka, 1971) Ch. 1, Sections 3, 4 [Translated into English 1st ed.: *Scattering, Reactions and Decays in Nonrelativistic Quantum Mechanics* (Jerusalem: Israel Program for Scientific Translations, 1969)]
16. Klimov A E, Shumskii V N *Prikl. Fiz.* (3) 74 (2004)
17. Kozhanov A E et al. *Fiz. Tekh. Poluprovodn.* **40** 1047 (2006) [*Semicond.* **40** 1021 (2006)]
18. Kristovskii K G et al. *Fiz. Tverd. Tela* **46** 123 (2004) [*Phys. Solid State* **46** 122 (2004)]
19. Akimov B A, Khokhlov D R *Semicond. Sci. Technol.* **8** S349 (1993)
20. Chesnokov S N et al. *Infrared Phys. Technol.* **35** 23 (1994)
21. Akimov B A et al. *Solid State Commun.* **66** 811 (1988)
22. Skipetrov E P, Nekrasova A N, Khorosh A G *Fiz. Tekh. Poluprovodn.* **28** 815 (1994) [*Semicond.* **28** 478 (1994)]

PACS numbers: 78.20.Hp, **76.80.+y**

DOI: 10.1070/PU2006v049n09ABEH006095

Modulation gamma-resonance spectroscopy

A V Mitin

1. Introduction

Thanks to the Mössbauer effect, the gamma range of electromagnetic waves is being mastered more and more in both fundamental and technological areas and is beginning to compete, in terms of its complexity of problems and exactness of measurements, with the optical range with its laser light sources [1, 2]. The standard Mössbauer spectroscopy is being replaced with gamma optics, an important part of which is the modulation gamma-resonance spectroscopy. The idea behind this spectroscopy is the possibility of controlling dynamical processes in matter by modulating a gamma resonance via external varying magnetic fields with frequencies exceeding the reciprocal lifetimes of excited states of Mössbauer nuclei (i.e., in the megahertz frequency range). This frequency range of dynamical processes covers the range of high-frequency fields of nuclear magnetic resonance (NMR), quadrupole. ferromagnetic, electron paramagnetic, and optical resonances. These perturbations are detected by measuring changes in gamma-resonance responses, which manifest themselves in distortions of the Mössbauer spectrum, such as shifts and the broadening of lines, and the emergence of satellite lines, the collapse of the hyperfine structure of lines under rapid magnetization reversal of ferromagnets, as well as in the onset of quantum beats caused by the interference of nuclear states.

But the intensities of the existing sources of gamma radiation (natural or synchrotron) are much lower than the values needed for producing inverse population in isomeric nuclear states. One encouraging fact here is the recently discovered nuclear excitation of ^{197}Au caused by an electron transition stimulated by the photoionization of the K-shell by X-ray radiation from a synchrotron source [3].

The modern method of theoretical analysis of gamma-resonance processes has had a great impact on the development of modulation gamma-resonance spectroscopy. The method combines the solution of the Maxwell equations in a medium and of the equations for the nuclear density matrix and showed its usefulness in examining processes accompanying the transmission of gamma radiation [4, 5]. However, to describe gamma-resonance scattering, I used a method for solving equations for the density matrix with second quantization of the gamma-radiation field [6, 7]. This approach has made it possible to solve problems related to the effect of alternating fields and relaxation on gamma resonances.

2. Ultrasonic modulation of gamma radiation

Already in their first Mössbauer experiments, Ruby and Bolef [8] recorded frequency modulation of gamma radiation with satellites whose distances from the spectral lines were found to be integer multiples of the ultrasonic frequency of the vibrating source or absorber of gamma radiation. However, the situation with a thick vibrating Mössbauer absorber was still unclear. The theory developed in Refs [1, 9, 10] showed that when the absorber or source vibrates with a frequency Ω, the intensity of gamma radiation is given by

$$P = \sum_{n=-\infty}^{\infty} J_n^2(k_1 a)\,\mathrm{Tr}\left\{ \exp\left(\mathrm{i}k_1 z\hat{b}_n\right)\hat{\chi}\exp\left(-\mathrm{i}k_1 z\hat{b}_n^{\dagger}\right)\right\}, \quad (1)$$

where k_1 is the wave number of the gamma radiation, a is the amplitude of the ultrasonic vibrations, z is the thickness of the absorber, J_n is the nth Bessel function, $\hat{b}_n$ is the tensor refractive index for a gamma wave with a shift in the gamma-radiation frequency by $n\Omega$, with Ω being the ultrasonic frequency, $\hat{\chi}$ is the polarization density matrix of the incident gamma radiation, and † stands for Hermitian conjugation.

If the source and absorber vibrate simultaneously with the same frequency and amplitude, the argument $k_1 a$ of the Bessel function can be replaced with the expression

$$w = 2k_1 a \sin\left\{\frac{1}{2}\left[\varphi_1 - \varphi_2 + \frac{\Omega}{2}(z_2 - z_1)\right]\right\}, \quad (2)$$

where $z_2 - z_1$ is the distance between the source and absorber and $\varphi_2 - \varphi_1$ is the difference between their ultrasonic phases.

These results were corroborated by subsequent theoretical works [11–13] and in experiments [14].

It follows from general considerations that ultrasonic vibrations cannot alter the polarization of gamma radiation. This fact, corroborated by experiments in analyzing the polarization properties of ultrasonic satellites [15], formed the basis for separating the effect of gamma magnetic resonance (GMR) from magnetostriction ultrasonic vibrations excited by a radio-frequency magnetic field (RFMF) [16]. We note that by this time (1982), ultrasonic modulation induced by an RFMF due to magnetostriction in ferromagnets became a widely accepted method in modulation gamma-resonance spectroscopy, work on which began in 1968 [17, 18]. In this connection, Baldokhin et al. [19] studied the ultrasonic modulation of the Mössbauer spectrum of the yttrium iron garnet (YIG) excited by an RFMF. The behavior of the YIG Mössbauer spectrum and its dependence on the size and direction of the constant magnetic field was explained on the basis of the assumption made in Ref. [19] that the vibrations of the walls of magnetic domains generate sound. Later, this mechanism was developed in Refs [20 – 22] and other works.

The next step in studying ultrasonic modulation was made in the experiment by Mishory and Bolef [23], in which the researchers discovered the effect of suppression of gamma-resonance self-absorption for high-powered ultrasound [23]. A theory in which the main role is played by relative (rather than absolute) strain (Fig. 1) produced results that were in good agreement with the data of this experiment (see Ref. [24]). It accounted for the spatial distribution of a standing ultrasonic wave over the thickness of the Mössbauer absorber. For a steady observation mode, it was assumed that the magnetic field strength of the gamma radiation can be represented as

$$h^p = \sum_{n=-\infty}^{\infty} h_n^p(z)\, \exp(\mathrm{i}n\Omega t)\,, \tag{3}$$

where the subscript $p = \pm 1$ determines the polarization of the left- and right-hand polarization components of the magnetic field strength of the gamma wave (the 14.4 KeV magnetic gamma transition in ^{57}Fe nuclei).

Then, if we move to the local harmonic system of coordinates via the transformation

$$h_n'^p(z) = \sum_{n'=-\infty}^{\infty} J_{n+n'}\left[k_1 a(z)\right] h_{n'}^p\,, \tag{4}$$

we obtain a system of equations describing the spatially inhomogeneous ultrasonic modulation of gamma radiation:

$$\frac{\mathrm{d}h_n'^p}{\mathrm{d}z} + \frac{1}{2}\, k_1 \frac{\mathrm{d}a(z)}{\mathrm{d}z}\left(h_{n+1}'^p - h_{n-1}'^p\right) = \mathrm{i}k_1 \sum_{p'=\pm 1} b_n^{pp'} h_n'^{-p'}\,, \tag{5}$$

where $b_n^{pp'}$ is the tensor refractive index of the nth harmonic.

The solution of system of equations (5) depends on the gradient of the index of ultrasonic modulation of gamma radiation, $k_1\, \mathrm{d}a/\mathrm{d}z$; this dependence allows developing the method known as ultrasonic Mössbauer introscopy [25, 26].

Further progress in the method of ultrasonic modulation of gamma resonance amounted to developing a new technique for detecting ultrasonic oscillations of gamma radiation [27]. A 'time – amplitude' converter was used to record quantum beats of gamma radiation. Initially, the theory proposed in [28], which dealt with the interference of gamma radiation, was described by a fairly complex formula. Later, however, this dependence was written in a form more compact (and more general) than in Ref. [28]; the formula for the intensity of the gamma radiation passing through a Mössbauer absorber also allowed for the hyperfine structure of Mössbauer nuclei and an arbitrary polarization of the incident radiation [29]:

$$P = \sum_{n,n'} \exp\left[\mathrm{i}n\left(\Omega t + \varphi\right)\right] J_{n'}(ka)\, J_{n'-n}(ka) \times \mathrm{Tr}\left\{\exp\left(\mathrm{i}kz\hat{b}_{n'-n}\right)\hat{\chi}\exp\left(-\mathrm{i}kz\hat{b}_{n'}^{\dagger}\right)\right\}. \tag{6}$$

We note that much experimental work went into studies of ultrasonic quantum beats: research on ^{129}I nuclei [30], analysis of spectra in the presence of relaxation [31], determination of the hyperfine parameters of Mössbauer nuclei [32], observation of coherent transition effects [33, 34], and the study of the effect of the absorber thickness on the phase of quantum beats [35, 36].

Very short gamma radiation pulses have been used to detect the gamma-echo effect, caused by the interference of the incident radiation and the ultrasonic modulated radiation. The latter develops much more slowly and is generated in a thick absorber [37, 38].

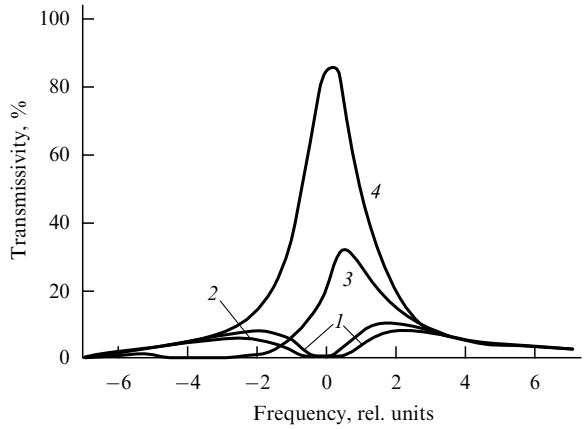

Figure 1. Frequency spectra of gamma-resonance self-absorption as functions of the ultrasound amplitude: *1*, 0; *2*, 0.5; *3*, 5; and *4*, 50 [24].

3. Gamma magnetic resonance

Gamma magnetic resonance, or GMR, played a key role in the development of modulation gamma-resonance spectroscopy. Before this effect was discovered, Bitter [39] and Pryce [40] studied radio-optical double resonance and predicted the possibility of observing magnetic resonance on the Zeeman electronic levels of the excited states of atoms populated by optical pumping. The same researchers showed that in a strong RFMF, the electron levels split into sublevels with the energy separation proportional to the RFMF strength. This theoretical work, successful experiments that corroborated these results, and the discovery of the Mössbauer effect prompted Hack and Hamermesh [41] to calculate the probability of a radiative transition from an excited state to the single-level ground state. The researchers also confirmed the possibility of RFMF splitting of nuclear Zeeman levels, but without estimating the possibility of observing this effect in experiments. Apparently for this reason, the first experiments by Matthias [42] on the effect of a resonant RFMF on the Mössbauer spectrum were fraught with errors, since the observed effect was due to ultrasonic modulation of gamma radiation caused by magnetostriction of the sample [43].

In 1966, the theory of gamma magnetic resonance came into being [44]. Such resonance is the effect of the excitation of Mössbauer gamma-resonance transitions between the Zeeman nuclear sublevels of the ground and excited states that occur simultaneously with NMR transitions stimulated by an RFMF inside isomeric states. The theory made it possible to calculate, in the two-photon approximation, the gamma photon and the RFMF photon, the cross section of Mössbauer absorption in a fine powder of metallic iron. A key factor was an estimate of the possibility of observing the GMR effect with the hyperfine enhancement of the RFMF on a nucleus in ferromagnets taken into account. Later, Heiman et al. [45] detected the GMR effect by using the gamma-resonance scattering method with the same sample, a fine powder of metallic iron, for which the possibility of observing GMR had been predicted earlier [44]. Yakimov et al. [46] and Vagizov et al. [47] observed GMR in paramagnets. But most informative were the experiments with ferromagnets in which gamma radiation was transmitted through an absorber (^{57}Fe in α-Fe) [48 – 50] and with iron – nickel alloys [51, 52]. Here, the researchers observed not only the quasienergy line broadening [48] but also line splitting [49 – 52] (Fig. 2).

Polarization methods for detecting GMR have also been developed. An earlier theoretical paper [53] studied the change in the polarization of gamma radiation caused by GMR excitation. Later, Chugunova and I proposed using the nuclear Faraday effect, birefringence, and the Malus law to observe GMR [54 – 56], and this was implemented by Leksin et al. [16] in an experiment in which GMR was detected on ^{57}Fe nuclei in iron in the source and absorbed with split hyperfine sublevels in constant magnetic fields.

Various aspects of observing the GMR effect in paramagnets in conditions of electron relaxation were studied in Refs [57, 58]. As a result of analysis, it has been found that when the electron relaxation rate is comparable to the spontaneous Mössbauer linewidth, the GMR effect weakens substantially. Hence, the experiments in which GMR was observed in paramagnets were conducted by Vagizov et al. [47] and Leksin et al. [48] at liquid nitrogen temperatures.

Meanwhile, the theory of the GMR effect was also being developed. It was found that stimulation of GMR is accompanied by magnetic quantum beats at frequencies that are integral multiples of the RFMF frequency [59]. Later, their spectra were thoroughly analyzed in [60] (Fig. 3). To describe the effect of GMR absorption in the case of a thin absorber, the following formula was derived:

$$P \sim \mathrm{Re} \sum_{Q=-2L}^{2L} \exp\left[\mathrm{i}Q(\Omega_1 t + \varphi)\right] \mathrm{Tr}\left\{\hat{\chi}\hat{B}_{Q,0}\right\}, \tag{7}$$

$$B_{Q,0}^{pp'} = \sum_{g_1,e_1} \sum_{M=-L}^{L} (pp')^{\varepsilon} \exp\left[\mathrm{i}(p-p')\psi\right] d_{p,M-Q}^{(L)}(\theta)\, d_{p',M}^{(L)}(\theta) \times \frac{S_{g_1,e_1}^{M-Q}(\beta_g,\beta_e)\, S^{M}(\beta_g,\beta_e)}{\mathrm{i}[e_1 a_e - g_1 a_g + M\Omega_1 - \Delta_1] + \Gamma/2}, \tag{7a}$$

$$S_{g_1,e_1}^{M-Q}(\beta_g,\beta_e) = \sum_{g,e} d_{g_1,g}^{(I_g)}(\beta_g)\, C(I_g L I_e; g, M-Q, e)\, d_{e,e_1}^{(I_e)}(-\beta_e). \tag{7b}$$

Here, $a_r \sin\beta_r = \omega_{1r}$ and $a_r \cos\beta_r = \omega_{0r} - \Omega_1$, with $r = g, e$; the superscript $\varepsilon = 0, 1$ determines the electric and magnetic gamma transition, respectively; Γ is the width of the spectra

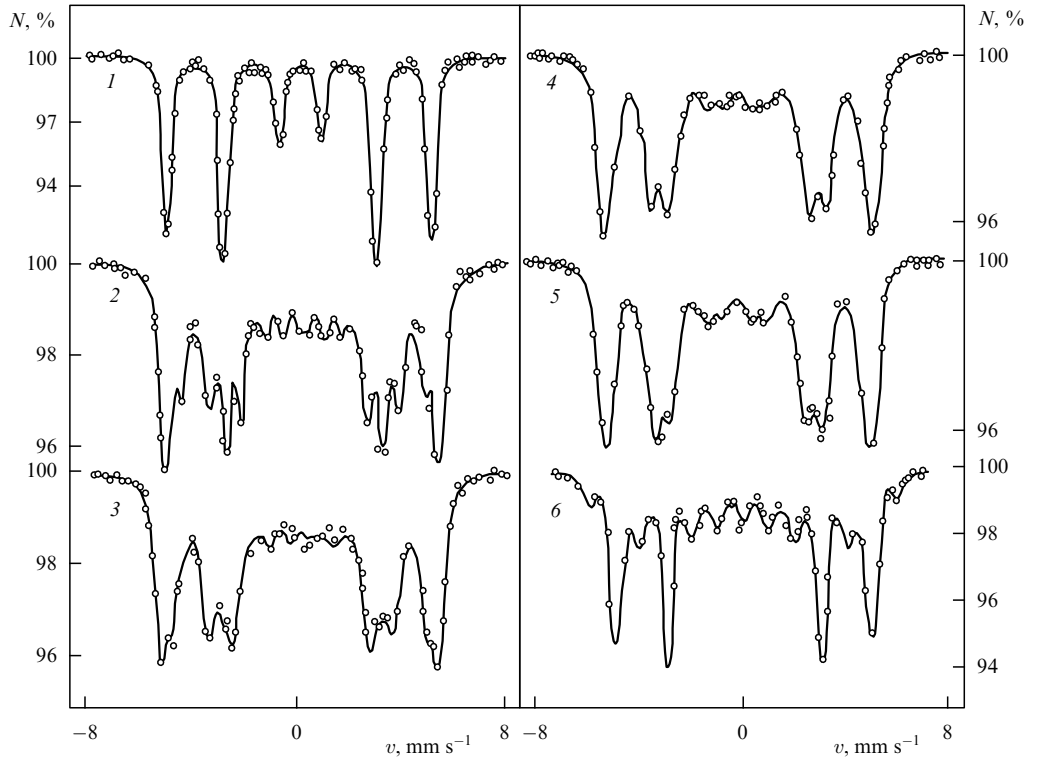

Figure 2. Mössbauer spectra for an α-Fe sample in the presence of a constant magnetic field at different frequencies [49]: *1*, $\nu = 0$; *2*, $\nu = 20$ MHz; *3*, $\nu = 22$ MHz; *4*, $\nu = 24$ MHz; *5*, $\nu = 26$ MHz; and *6*, $\nu = 36$ MHz; $H_1 \approx 25-30$ Oe; N is the relative gamma-photon counting rate.

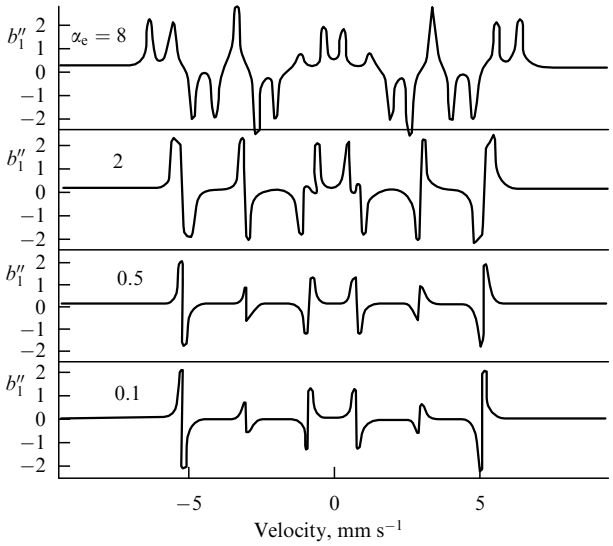

Figure 3. Doppler spectra of the imaginary part of the first GMR harmonic [60]. The dependence on the effective field on the nucleus is $\alpha_e = 2g\beta_N H_1/(\hbar\Gamma)$, and b_1'' is the imaginary part of the pseudosusceptibility of the first harmonic of the gamma-radiation intensity.

lines of the Mössbauer absorber; and the subscripts e and g denote the quantum numbers of the excited and ground isomeric states of the nucleus, respectively. The notation for other symbols is standard (e.g., see Ref. [61]). Equation (7) shows that the maximum order of the harmonics of the magnetic quantum beats in this absorber is limited by $2L$, where L is the multipole order of the gamma transition, in contrast to, generally speaking, the unlimited order of harmonics of the quantum beats in the case of ultrasonic modulation.

Equations (7), (7a), and (7b) have been derived under the assumption that the gamma radiation and the RFMF act on the ground and excited states of the nucleus simultaneously due to the coherent nature of the forward-scattered gamma wave. Hence, interference of the magnetic quasienergy isomeric state occurs. The problem was in the approximation of a resonant rotating field, and the effect should manifest itself when the g-factors of the isomeric states are of the same sign and the Rabi frequencies are comparable to the difference between the Larmor frequencies [61 – 63]. Voitovetskii et al. [64] were able to observe the isomeric interference effect in their experiments with GMR on ^{181}Ta nuclei in tantalum. Recently, it was found (see Ref. [65]) that the intensity of the first harmonic with GMR excited on ^{181}Ta nuclei is at its maximum when the RFMF frequency is selected in the interval between the values of the nuclear Larmor frequencies of the ground and excited states.

When the nuclear g-factors in the ground and excited states of the nucleus have different signs, as in the case of ^{57}Fe, isomeric interference emerges due to the components of the oscillating RFMF that rotate in opposite directions [61], with the effect caused by the quantum transitions for which the magnetic quantum numbers obey the condition $e + g = 0$. A theory of GMR scattering was developed much later than the experimental data were gathered. The first works were Refs [66, 67], but a complete theory [68–71] emerged later. A more general theory was built in Refs [70 – 72], from which the formulas describing radio-optical double resonance (among other things) follow [73]. In Refs [70, 71], I described polarization of gamma radiation and calculated the spectra of GMR scattering. Interference of the scattering amplitudes of quasienergy states has also been discovered [2, 74]. Such interference manifests itself much more strongly than the interference of the hyperfine scattering amplitudes. This research was continued by Sadykov et al. [75, 76], who studied quantum interference in the electron – nucleus system of levels.

Today, there is an upsurge of interest in the problem of using the interference of quantum states that are induced by high-frequency fields with the aim of creating conditions for resonance transparency of the medium [77]. However, in contrast to the intensities of the optical range of electromagnetic radiation, in which substantial population of the excited states can be achieved due to the existence of high-power lasers, the intensities of natural and synchrotron radiation of gamma radiation are too low for the isomeric nuclear states to become populated. At the same time, Mössbauer nuclei, which carry a magnetic moment, can interact very strongly with an RFMF by exciting GMR. The problem therefore emerged of stimulating GMR by a bi-radio-frequency coherent field with frequencies that simultaneously and resonantly excite the ground and excited isomeric states of the nucleus.

Using a ^{57}Fe nucleus in iron as an example, Roganov and I examined (see Ref. [78]) the situation where the gamma-radiation frequency was shifted by the half-sum or half-difference of the frequencies of a bi-radio-frequency field. Later, this condition was replaced by a more general one, which was determined by the structure of the symmetry group of the harmonics of the spin states of gamma transitions [79].

Analysis showed that in a thick absorber, the resonance spectrum has a much more distinct structure of the quantum-beat harmonics than in the case of time-independent detection (Fig. 4). Preliminary studies of excited GMR harmonics on ^{181}Ta nuclei in tantalum but at a single RFMF frequency also exhibit a large resonant transparency of the Mössbauer medium for quantum beats. Hence, the effect of quantum beats stimulated by GMR may find applications in integrated gamma-optics elements and, similarly to X-ray radiation [80], in developing circuits in which control and amplification are done by gamma radiation.

One of the possible areas in which GMR can be used is the study of disordered magnetic materials. The need to develop such methods stems from studies of magnetic amorphous and nanocrystalline materials whose Mössbauer spectra are characterized by strong inhomogeneous broadening and are similar for different chemical compositions. The idea of using GMR consists in the following [62, 63]. Gamma radiation from a source with a natural linewidth Γ interacts only with a small fraction of nuclei that are in an inhomogeneous hyperfine magnetic field with the width $\sigma \gg \Gamma$. The pumping RFMF H_1 acting on the nucleus forms an effective field with the amplitude

$$H_{\text{eff}} = \left[\left(H_{\text{hf}} - \frac{\hbar\Omega_1}{g_r\beta_N}\right)^2 + H_1^2\right]^{1/2}, \qquad (8)$$

where H_{hf} is the hyperfine field on the nucleus, g_r is the g-factor of the excited ($r = e$) or ground ($r = g$) states, and β_N is the nuclear Bohr magneton. The frequency Ω_1 of the strong RFMF is resonant only for a specific spin packet. Hence, only for the given spin packet does there emerge a quasienergy system of levels. The weak scanning field H_2 with a frequency

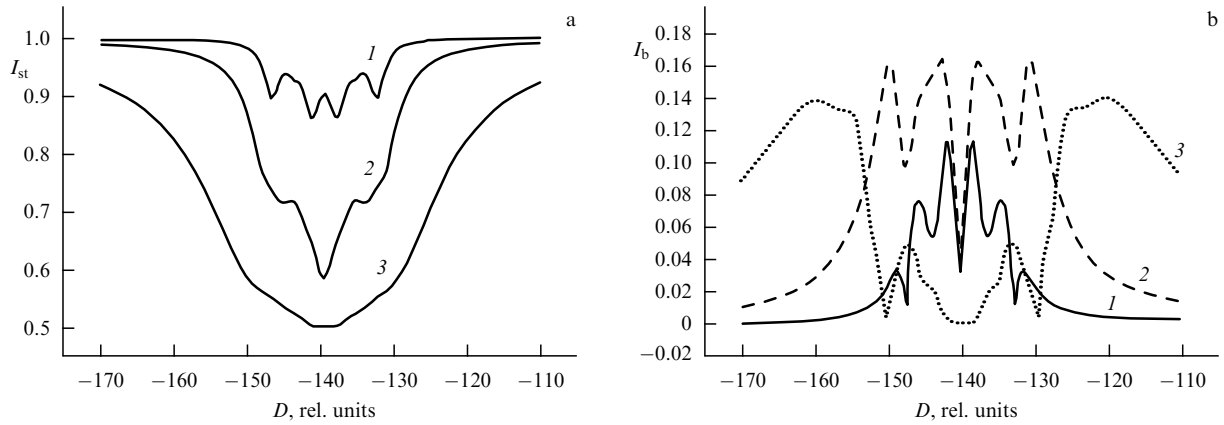

Figure 4. GMR bi-radio-frequency spectra, the symmetric case. Dependence on the thickness s of the absorber [79]: (a) time-independent intensity (curve *1*, $s = 1$; curve *2*, $s = 10$; and curve *3*, $s = 100$). (b) Intensity of the b-harmonic (curve *1*, $s = 1$; curve *2*, $s = 10$; and curve *3*, $s = 100$). D is the frequency tuning of gamma radiation in units of $\Gamma/2$.

Ω_2 is capable of exposing these quasienergy states. A further modification of this method [81] was based on using a low-frequency modulation of the amplitude of the pumping RFMF (transverse modulation) and of the constant magnetic field (longitudinal modulation). Analysis has shown, for instance, that the spectrum of the second harmonic at the frequency Ω_2 has narrow lines despite a substantial spread of the hyperfine fields [82, 83] (Fig. 5).

The results of these studies are awaiting their application in the case of synchrotron gamma radiation. Further progress is expected as these methods are extended to nanostructures.

In concluding this section, I note the possibility of using the method of GMR magnetic quantum beats for verifying the T-invariance of nuclei with mixed M1–E2 gamma transitions [84].

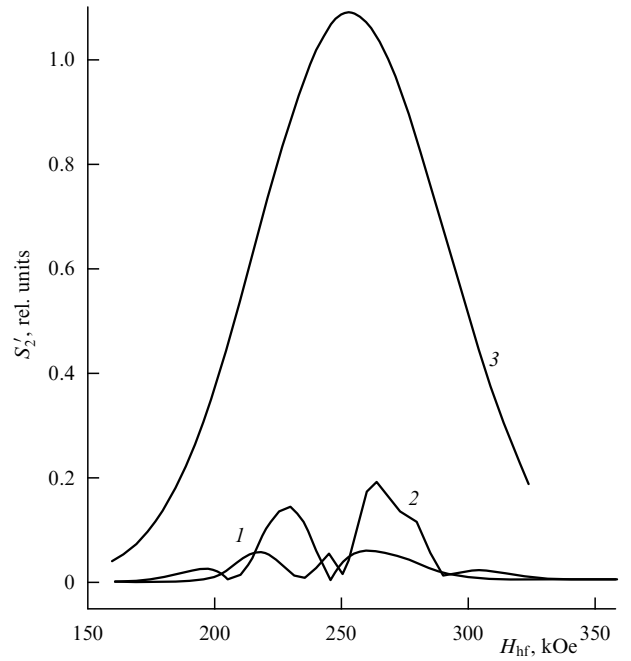

Figure 5. Distribution of the square of the absolute value of the second modulation harmonic, integrated over the frequency spectrum of gamma radiation, as a function of the hyperfine field strength H_{hf} ($\omega_{0e}/2\pi = 19.91$ MHz, $\omega_{1e}/2\pi = 2.5$ MHz, and $\Omega_2 = 3$ MHz) at $\Omega_1/2\pi = 17.91$ MHz (curve *1*) and at $\Omega_1/2\pi = 21.91$ MHz (curve *2*). Curve *3* is the Gaussian function $g(H_{hf})$ of the distribution of the hyperfine field in an amorphic metal alloy, $H_{hf}^0 = 255$ kOe [83].

4. Radio-frequency, microwave, and optical double gamma resonances

The main idea of most suggestions concerning modifications of the gamma resonance approach has amounted to simultaneous excitation of nuclear magnetic, ferromagnetic, electron paramagnetic, and optical resonances [85]. But it has been found that substantially changing a gamma resonance is fraught with many difficulties in experiments. The reason is that very powerful sources of radiation are needed to observe the effect, and low temperatures are needed to guarantee a sizable difference in populations of the ground and excited electron states. However, in ferromagnets with an RFMF whose amplitude was significantly larger than the coercive force and whose frequency was several times higher than the Larmor frequencies of the ground and excited states of the nucleus, Pfeiffer [86] observed a collapse of the hyperfine structure of the Mössbauer spectrum induced by permalloy foil in a strong RFMF field of 15 Oe. In this case, an increase in the RFMF frequency up to 106 MHz was found to lead to a collapse of the Mössbauer spectrum into a single line. The interpretation of this effect is similar to that of spectral narrowing of magnetic-resonance lines caused by molecular motion. Later, other researchers also observed the collapse of the hyperfine structure of the Mössbauer spectrum. I note that Kopcewicz et al. [87] used this effect to determine quadrupole splitting.

The effect of pulsed magnetization reversal on the gamma resonance was studied by analyzing the responses to synchrotron radiation of a $FeBO_3$ single crystal, in the geometry of Bragg scattering [88], and in the passage of radiation through the sample [89].

However, in view of the above-noted difficulties, it has proved extremely difficult to observe such effects in paramagnets by exciting EPR transitions. Nevertheless, Cherepanov et al. [90] were able to observe the broadening of K-lines of the Mössbauer spectrum of a single crystal of aluminum nitrate alloyed with iron placed in a microwave magnetic field of the frequency 9.41 GHz with the amplitude 0.7 Oe.

Earlier, theorists examined the possibility of light affecting Mössbauer spectra. The researchers assumed that such

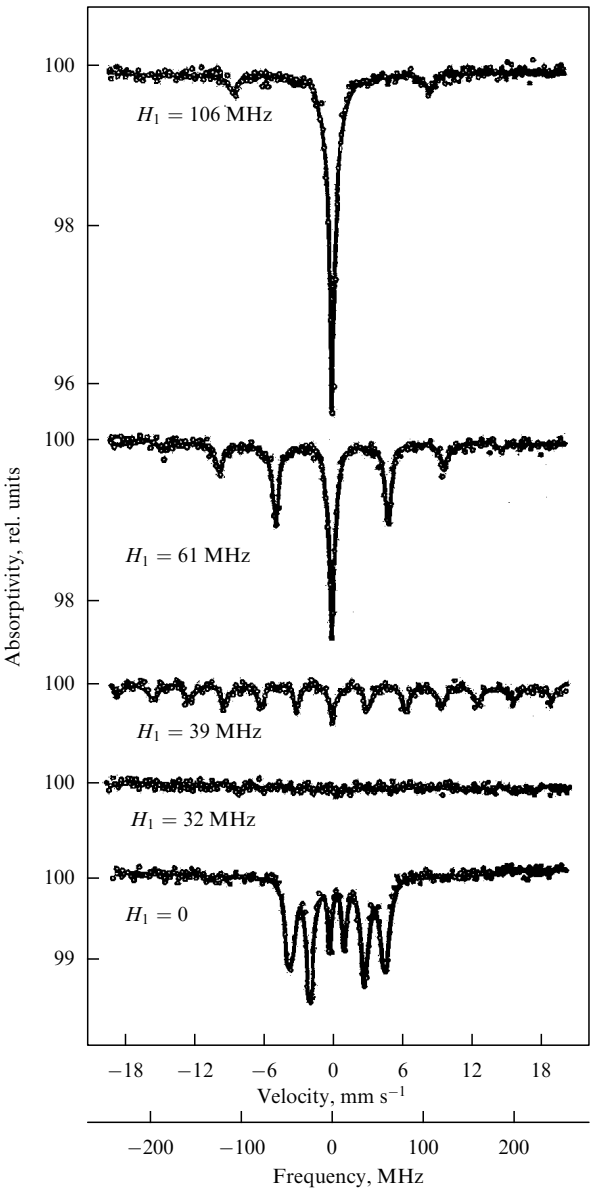

Figure 6. The RFMF collapse effect as a function of the applied frequency [86].

effects would manifest themselves in changes in the chemical shift [91], the quadrupole [92] and magnetic [93, 94] hyperfine interactions, and the presence of the laser effect of 'burning' of narrow resonances in the Doppler-broadened line of gamma transitions in gases [95].

Experimenters were able to observe an increase in the quadrupole splitting and a decrease in the isomeric shift on semiconductors [96], as well as a redistribution of intensities of the spectral lines in yttrium gallium garnets [97]. Such investigations were continued by recent experiments in which the quadrupole interaction of $^{151}Eu^{3+}$ in a number of single crystals was changed [98] and a vibrational 'ring' was recorded after a laser pulse acted on the gamma resonance of ^{57}Fe in MgO [99].

5. Conclusion

Summarizing the results of modulation gamma-resonance spectroscopy, we can say that the prospects of it becoming nonlinear gamma-resonance spectroscopy are great. However, this will not happen very soon, because powerful synchrotrons and other sources of electromagnetic radiation in the energy range from 10 to 30 keV must be built. Apparently, in the next decade, research will remain focused on the above effects of modulation gamma-resonance spectroscopy. Today, this research is being done in Russia (Kazan, Nizhni Novgorod, Moscow), USA (Texas), Belgium (Louvain), Romania (Bucharest), and other countries, which makes it possible to believe that new results and applications will come very soon.

References

1. Makarov E F, Mitin A V *Usp. Fiz. Nauk* **120** 55 (1976) [*Sov. Phys. Usp.* **19** 741 (1976)]
2. Mitin A V *Izv. Ross. Akad. Nauk, Ser. Fiz.* **62** 395 (1998) [*Bull. Russ. Acad. Sci., Ser. Phys.* **62** 323 (1998)]
3. Kishimoto S et al. *Phys. Rev. Lett.* **85** 1831 (2000)
4. Mitin A V *Phys. Status Solidi B* **53** 93 (1972)
5. Mitin A V *Phys. Lett. A* **84** 278 (1981)
6. Mitin A V *Phys. Lett. A* **84** 283 (1981)
7. Mitin A V *Opt. Spektrosk.* **53** 288 (1982) [*Opt. Spectrosc.* **53** 168 (1982)]
8. Ruby S L, Bolef D I *Phys. Rev. Lett.* **5** 5 (1960)
9. Mitin A V *Kvant. Elektron.* **3** 840 (1976) [*Sov. J. Quantum Electron.* **6** 458 (1976)]
10. Mitin AV, in *Proc. of the XX Colloquium Spectroscopy Intern.: CSI and 7th Intern. Conf. on Atomic Spectroscopy: ICAS, Prague, Czechoslovakia, 1977, Invited Lectures*, p. 461
11. Ognjanov N I, Tsankov L T *J. Phys.* (Paris) **44** 859 (1983)
12. Ognjanov N I, Tsankov L T *J. Phys.* (Paris) **44** 865 (1983)
13. Dzyublik A Ya *Phys. Status Solidi B* **134** 503 (1986)
14. Lobko A S, Rubatskaya E E *Pis'ma Zh. Tekh. Fiz.* **16** 46 (1990)
15. Leksin V V et al. *Fiz. Tverd. Tela* **22** 1509 (1980) [*Sov. Phys. Solid State* **22** 881 (1980)]
16. Leksin V V, Manapov R A, Mitin A V *Fiz. Tverd. Tela* **24** 906 (1982)) [*Sov. Phys. Solid State* **24** 514 (1982)]
17. Heiman N D, Pfeiffer L, Walker J C *Phys. Rev. Lett.* **21** 93 (1968)
18. Asti G, Albanese G F, Bucci C *Nuovo Cimento B* **57** 531 (1968)
19. Baldokhin Ya V et al. *J. Phys. Colloq.* (Paris) **33** C6-145 (1972)
20. Mitin A V, Tarasov V A *Zh. Eksp. Teor. Fiz.* **72** 793 (1977) [*Sov. Phys. JETP* **45** 414 (1977)]
21. Turov E A, Lugovoi A A *Fiz. Met. Metalloved.* **50** 717, 903 (1980)
22. Lugovoi A A, Turov E A, Dyakin V V *Fiz. Met. Metalloved.* **60** 1124 (1985)
23. Mishory J, Bolef D I, in *Mössbauer Effect Methodology: Proc. of the Symp.* Vol. 4 (New York: Plenum Press, 1968) p. 13
24. Mitin A V *Fiz. Tverd. Tela* **20** 1626 (1978) [*Sov. Phys. Solid State* **20** 941 (1978)]
25. Mitin A V *Solid State Commun.* **39** 1087 (1981)
26. Mitin A V *Phys. Status Solidi B* **113** 113 (1982)
27. Perlow G J *Phys. Rev. Lett.* **40** 896 (1978)
28. Monahan J E, Perlow G J *Phys. Rev. A* **20** 1499 (1979)
29. Mitin A V, in *Tezisy 2-go Vsesoyuz. Simp. po Svetovomu Ekho, Kazan', 17–19 Iyunya 1981 g.* (Digest of 2nd All-Union Symp. Photon Echo, Kazan, June 17–19, 1981) (Ed. I Kh Khaduev) (Kazan: AN SSSR, Kazanskii Filial, 1981) p. 73
30. Zhang Gui-Lin, Du Marchie Van Voorthuysen E H, De Waard H *Phys. Lett. A* **91** 417 (1982)
31. Salkola M, Javanainen J, Katila T *Hyperfine Interact.* **29** 1559 (1986)
32. Hollatz R, Rüffer R, Gerdau E *Hyperfine Interact.* **42** 1141 (1988)
33. Helistö P et al. *Phys. Rev. Lett.* **49** 1209 (1982)
34. Helistö P et al. *Hyperfine Interact.* **29** 1563 (1986)
35. Shvyd'ko Yu V, Smirnov G V *J. Phys.: Condens. Matter* **4** 2663 (1992)
36. Popov S L et al. *Europhys. Lett.* **28** 439 (1994)
37. Helistö P et al. *Phys. Rev. Lett.* **66** 2037 (1991)
38. Smirnov G V, Potzel W *Hyperfine Interact.* **123/124** 633 (1999)
39. Bitter F *Phys. Rev.* **76** 833 (1949)
40. Pryce M H L *Phys. Rev.* **77** 136 (1950)
41. Hack M N, Hamermesh M *Nuovo Cimento* **19** 546 (1961)

42. Matthias E, in *Hyperfine Structure and Nuclear Radiation*: *Proc. of a Conf., USA, August 25–30, 1967* (Eds E Matthias, D A Shirley) (Amsterdam: North-Holland, 1968) p. 815
43. Pfeiffer L, Heiman N D, Walker J C *Phys. Rev. B* **6** 74 (1972)
44. Mitin A V *Zh. Eksp. Teor. Fiz.* **52** 1596 (1967) [*Sov. Phys. JETP* **25** 1062 (1967)]
45. Heiman N D, Walker J C, Pfeiffer L *Phys. Rev.* **184** 281 (1969)
46. Yakimov S S et al. *Pis'ma Zh. Eksp. Teor. Fiz.* **26** 16 (1977) [*JETP Lett.* **26** 13 (1977)]
47. Vagizov F G, Manapov R A, Mitin A V *Opt. Spektrosk.* **51** 941 (1981) [*Opt. Spectrosc.* **51** 522 (1981)]
48. Leksin V V, Manapov R A, Mitin A V *Izv. Akad. Nauk SSSR, Ser. Fiz.* **50** 2362 (1986)
49. Vagizov F G *Hyperfine Interact.* **61** 1359 (1990)
50. Vagizov F G *Hyperfine Interact.* **95** 85 (1995)
51. Tittonen I et al. *Phys. Rev. Lett.* **69** 2815 (1992)
52. Lippmaa M et al. *Phys. Rev. B* **52** 10268 (1995)
53. Mitin A V, in *Nekotorye Voprosy Magnitnoi Radiospektroskopii i Kvantovoi Akustiki*: *Materialy Nauchnoi Konf., Mai 1967, Kazan'* (Some Aspects of Magnetic Radio-Frequency Spectroscopy and Quantum Acoustics. Proc. of a Scientific Conf., May, 1967, Kazan) (Eds B M Kozyrev, U H Kopvillem) (Kazan: KFTI AN SSSR, 1968) p. 120
54. Mitin A V, Chugunova G P *Fiz. Tverd. Tela* **16** 614 (1974) [*Sov. Phys. Solid State* **16** 403 (1974)]
55. Chugunova G P, Mitin A V *Phys. Lett. A* **47** 243 (1974)
56. Mitin A V, Chugunova G P *Phys. Status Solidi A* **28** 39 (1975)
57. Bersuker I B, Borshch S A, Ogurtsov I Ya *Fiz. Tverd. Tela* **15** 2270 (1973) [*Sov. Phys. Solid State* **15** 1518 (1974)]
58. Mitin A V, Polyakov N V *Phys. Status Solidi B* **115** 477 (1983)
59. Mitin A V, in *Proc. of the 5th Intern. Conf. on Mössbauer Spectroscopy, Bratislava, 3–7 September, 1973* (Praha: Czechoslovakia Atomic Energy Commission. Nuclear Information Centre, 1975) p. 615
60. Mitin A V *Phys. Lett. A* **84** 278 (1981)
61. Mitin A V *Izv. Ross. Akad. Nauk, Ser. Fiz.* **56** (7) 186 (1992) [*Bull. Russ. Acad. Sci., Ser. Phys.* **56** 1108 (1992)]
62. Mitin A V, Makarov E F, Polyakov N V *Zh. Eksp. Teor. Fiz.* **90** 1931 (1986) [*Sov. Phys. JETP* **63** 1130 (1986)]
63. Mitin A V, Polyakov N V *Phys. Lett. A* **114** 27 (1986)
64. Voitovetskii V K et al. *Pis'ma Zh. Eksp. Teor. Fiz.* **36** 322 (1982) [*JETP Lett.* **36** 393 (1982)]
65. Mitin A V, Lyubimov V Yu, Sadykov E K *Pis'ma Zh. Eksp. Teor. Fiz.* **81** 538 (2005) [*JETP Lett.* **81** 424 (2005)]
66. Bashkirov Sh Sh, Sadykov E K *Fiz. Tverd. Tela* **20** 3444 (1978) [*Sov. Phys. Solid State* **20** 1988 (1978)]
67. Bashkirov Sh Sh, Belyanin A L, Sadykov E K *Phys. Status Solidi B* **93** 437 (1979)
68. Dzyublik A Ya *Phys. Status Solidi B* **104** 81 (1981)
69. Afanas'ev A M, Aleksandrov P Ya, Yakimov S S, Preprint IAE-3337/9 (Moscow: I V Kurchatov Institute of Atomic Energy, 1980)
70. Mitin A V *Phys. Lett. A* **84** 283 (1981)
71. Mitin A V *Opt. Spektrosk.* **53** 288 (1982) [*Opt. Spectrosc.* **53** 168 (1982)]
72. Mitin A V, Doctoral Thesis of Physico-Mathematical Sciences (Kazan: Kazan Physical-Technical Institute of the USSR Academy of Sciences, 1984)
73. Aleksandrov E B *Usp. Fiz. Nauk* **107** 595 (1972) [*Sov. Phys. Usp.* **15** 436 (1973)]
74. Mitin A V, in *Tezisy Vsesoyuz. Soveshchaniya po Yaderno-Spektroskopicheskim Issledovaniyam Sverkhtonkikh Vzaimodeistvii, Moskva, 1985* (Digest of All-Union Conf. on Nuclear Spectroscopy Studies of Hyperfine Interactions, Moscow, 1985) (Moscow, 1985) p. 110
75. Sadykov E K, Zakirov L L, Yurichuk A A *Laser Phys.* **11** 409 (2001)
76. Sadykov E K et al. *Izv. Ross. Akad. Nauk, Ser. Fiz.* **67** 995 (2003) [*Bull. Russ. Acad. Sci., Ser. Phys.* **67** 1099 (2003)]
77. Harris S E *Phys. Today* **50** (7) 36 (1997)
78. Mitin A V, Roganov D F *Izv. Ross. Akad. Nauk, Ser. Fiz.* **65** 941 (2001) [*Bull. Russ. Acad. Sci., Ser. Phys.* **65** 1020 (2001)]
79. Mitin A V, Aniskin I P, Tarasov V A *Izv. Ross. Akad. Nauk, Ser. Fiz.* **69** 1414 (2005) [*Bull. Russ. Acad. Sci., Ser. Phys.* **69** 1585 (2005)]
80. Dabagov S B *Usp. Fiz. Nauk* **173** 1083 (2003) [*Phys. Usp.* **46** 1053 (2003)]
81. Mitin A V *Phys. Lett. A* **213** 207 (1996)
82. Mitin A V, in *Proc. First Intern. Induced Gamma Emission Workshop 1997, Predeal, Romania* (Eds I I Popescu, C A Ur) (Bucharest: IGE Foundation, 1999) p. 145
83. Mitin A V *Opt. Spektrosk.* **92** 432 (2002) [*Opt. Spectrosc.* **92** 389 (2002)]
84. Mitin A V, Aniskin I P, in *Proc. of 7th AFOSR Workshop on Isomers and Quantum Nucleonics, Dubna, June 26–July 1, 2005*: *Book Abstracts* (Eds S A Kamarin, J J Carroll, E A Cherepanov) (Dubna: JINR, 2006) p. 206
85. Poole C P (Jr.), Farach H A *J. Magn. Res.* **1** 551 (1969)
86. Pfeiffer L *J. Appl. Phys.* **42** 1725 (1971)
87. Kopcewicz M, Wagner H-G, Gonser U *Solid State Commun.* **48** 531 (1983)
88. Shvyd'ko Yu V et al. *Phys. Rev. B* **52** R711 (1995)
89. Shvyd'ko Yu V et al. *Phys. Rev. Lett.* **77** 3232 (1996)
90. Cherepanov V M et al., in *Proc. of the First Intern. Induced Gamma Emission Workshop, Predeal, Romania* (Eds I I Popescu, C A Ur) (Bucharest: IGE Foundation, 1999) p. 394
91. Bersuker I B, Kovarskii V A *Pis'ma Zh. Eksp. Teor. Fiz.* **2** 286 (1965) [*JETP Lett.* **2** 182 (1965)]
92. Bashkirov Sh Sh, Sadykov E K *Pis'ma Zh. Eksp. Teor. Fiz.* **3** 240 (1966) [*JETP Lett.* **3** 154 (1966)]
93. Mitin A V *Fiz. Tverd. Tela* **10** 3632 (1968) [*Sov. Phys. Solid State* **10** 2880 (1969)]
94. Ivanov A S, Kolpakov A V, Kuz'min R N *Fiz. Tverd. Tela* **16** 1229 (1974) [*Sov. Phys. Solid State* **16** 794 (1974)]
95. Letokhov V S *Phys. Rev. A* **12** 1954 (1975)
96. Bashkirov Sh Sh et al. *Pis'ma Zh. Eksp. Teor. Fiz.* **27** 486 (1978) [*JETP Lett.* **27** 457 (1978)]
97. Bibikova Yu F et al. *Fiz. Tverd. Tela* **22** 2349 (1980)
98. Olariu S et al., in *Intern. Conf. of the Applications of the Mössbauer Effect*: *ICAME 2005, Montpellier, France, September 5–9, 2005*, Abstracts, p. T6–P17
99. Vagizov F et al., in *Intern. Conf. of the Applications of the Mössbauer Effect*: *ICAME 2005, Montpellier, France, September 5–9, 2005*, Abstracts, p. T6–P29

PACS numbers: **07.60.–j**, **87.64.–t**

DOI: 10.1070/PU2006v049n09ABEH006096

Methods and tools for the express immunoassay. A new approach to solving the problem

V E Kurochkin

1. Introduction

The rapid development of heterogeneous immunoassay (HetIA) techniques is facilitated by the high specificity of the antigen (Ag)–antibody (At) reaction underlain by the ability of the two molecules to recognize each other in a 'lock and key' fashion. Theoretically, it allows detecting a single molecule (particle) of the study substance in a real-time scale, provided highly sensitive assay methods are available for the purpose along with a mechanism to achieve a rapid transfer of individual Ag to the active centers immobilized at the surface. The practical solution to this problem is paramount for epidemiology, faced with the necessity of identifying causal factors of dangerous infections in multi-component environmental samples.

The proposed concept of the construction of highly sensitive systems for express immunoanalysis is first and

foremost based on the results of research conducted along the following three lines:

1. Purpose-oriented application of physical processes proceeding in the field of an ultrasound standing wave (USSW) for the transport of Ag to the immunosorbent (IS) surface under diffusion and concentration constraints imposed on mass transfer and for the minimization of effects of non-specific sorbing impurities.

2. Development of theoretical propositions of reflection photometry in application to thin-layer optically transparent elements (chemo- and biosensors) for the creation of highly sensitive detectors operating in a real-time regime and optimally fit to the reaction block.

3. Investigation into characteristics of the recurrent stochastic algorithm for processing 'linear trend' signals for the rapid and noise-independent assessment of informative parameters of the signals.

2. Intensification of antigen – antibody reactions using the standing wave of an ultrasonic field

Analysis of different methods for the acceleration of mass-transfer in HetIA has demonstrated that the use of traditional techniques such as a flow regime, intensification of mixing, etc. gives poor results [1 – 3]. The application of ultrasound (US) fields appears more promising, and the author believes that carrying out Ag – At reactions in a noncavitating USSW field of the megahertz range affords significant advantages because it permits

• forming IS layers with a 1/2 US-wavelength periodicity (using the radiation force action on IS particles) [4 – 6];

• retaining suspended IS particles in an US cell in the flow regime by counteracting the Stokes force to be able to change solutions of ingredients [7];

• ensuring noncontact free mixing in microsamples with a given spatial scale L ($L \gg \lambda$ for convective flows, $L \sim \lambda/2$ for Rayleigh flows and $L = (\lambda/4)\,2\delta$ for Schlichting boundary flows, where $\delta = (\nu/\pi f)^{1/2}$ is the width of the acoustic boundary layer, ν is the kinematic viscosity of the liquid, and f is the oscillation frequency [8]). The boundary layer width under ordinary conditions (water, temperature 20 °C) and $f = 3$ MHz is $\delta \sim 0.3$ μm.

The author of this publication has forwarded a hypothesis that the purpose-oriented creation of the Rayleigh flow or a combination of the Rayleigh and Schlichting flows may lay the basis for a new universal and rapid mechanism of Ag transfer to the IS surface. A flow speed proportional to the average acoustic energy E [8] (hence, controllable in a broad range) should be chosen in order (a) to substantially increase the velocity of mass transfer, i.e., the probability of the meeting of Ag and At; (b) not to interfere with specific interactions (in other words, the kinetic energy of Ag must be smaller than the Ag – At coupling energy); (c) to decrease the probability of nonspecific interactions between sample components and the IS surface; and (d) to ensure rapid and efficient removal of nonspecifically sorbed components of the sample at the wash-out stage.

For Ag of bacterial origin, USSW allows realizing an additional mechanism, that is, Ag transfer to the IS surface under the effect of radiation forces, which results in the concentration of particles at pressure nodes and antinodal points (depending on the medium and particle properties). The efficiency of such a mechanism increases with increasing the size of the particles. (At a certain ratio of densities and compressibilities of the particles and the medium, this mechanism may slow down and even completely block particle transfer by acoustic flows.)

The experimental arrangement used to verify the above hypothesis and the possibility of practical realization of the proposed mechanism are depicted in Fig. 1. It consists of two blocks, one for specific reactions at IS microspheres and the other for fluorescence detection. The former block includes an US-emitter, removable reaction microchambers (15, 20, and 25 μl), pumps for the introduction of reaction ingredients, and a thermostatic liquid. A microchamber is installed in the focus of objective lens *11* (see Fig. 1) that serves to feed a beam of exciting radiation onto reaction products and to collect an informative signal.

The working parameters of the device are $f = 1$ – 4 MHz, $E = 1 - 10$ J m^{-3}, and the pumping speed $u = 0.02$ – 0.50 cm s^{-1}.

The immunosorbent is prepared from optically transparent agarose or sepharose spherical beads of radius $R = 15$ μm.

In preliminary studies, the dependence of particle retention on E, f, u, and R was evaluated and optimal conditions were chosen for the complete retention of IS particles in the flow at the bulk velocity up to 1 ml min^{-1}. Methods were developed for the formation of a desired number of compact IS monolayers ($\geqslant 1$) parallel to the emitter plane in one- and two-wave US-chambers.

The efficiency of the proposed mechanism for the intensification of Ag – At reactions was assessed by comparing analytical characteristics obtained in analyses using the USSW technique and a traditional method [9], i.e., mixing by repeated pipetting on a microplate. The principal analytical

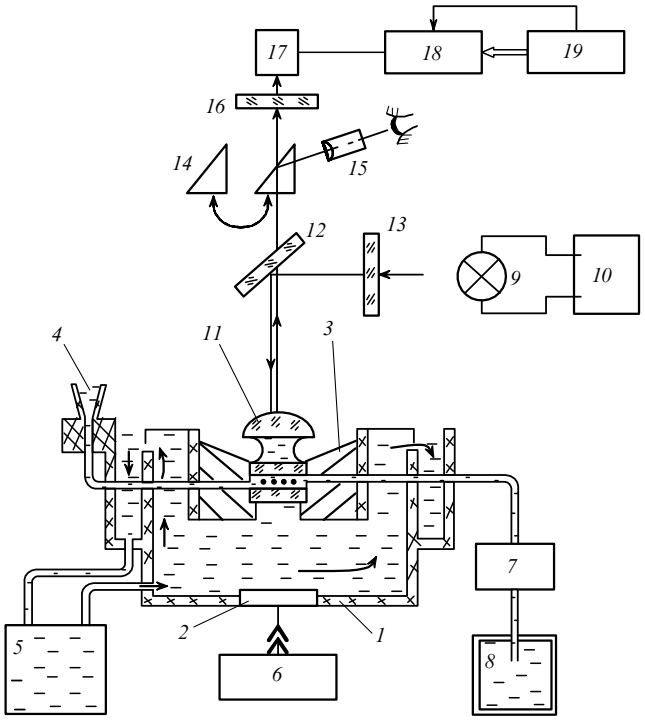

Figure 1. Diagram of experimental set-up: *1* — support of the US-emitter, *2* — US-emitter, *3* — microchamber, *4* — microfunnel, *5* — pump with a thermostat, *6* — high-frequency generator (HFG), *7* — peristaltic pump, *8* — container, *9*, *10* — radiation source, *11* — objective lens, *12*, *13*, *16* — light filters, *14* — rotary prism, *15* — eye-piece, *17* — photoelectronic multiplier (PEM), *18* — analog-digital converter (ADC), *19* — computer.

characteristics include the time necessary for the reaction to be completed (t_p), the duration of the wash-out procedure (t_o), and the sensitivity or detection limit (DL). The antigens being studied differ in size (immunoglobulins, toxins, viruses, and bacteria).

The results of experiments indicate that t_p depends on antigen dimensions (Fig. 2a), but even in the 'worst case' (large Brucella bacteria), the use of a US-field allows t_p to be reduced 25-fold (to less than 90 s) compared with the reaction time in the traditional method (curve *3* in Fig. 2a and the curve in Fig. 2b, respectively).

The use of US-fields not only permits diminishing t_p but also makes the wash-out procedure for the removal of non-specifically absorbed impurities three times shorter. This result is achieved by combining the flow regime and the action of acoustic boundary flows (Fig. 2a).

The applicability of the method in question for practical purposes was checked by assaying coded samples that contained the threshold or higher concentrations of heterologous microorganisms and toxins as impurities, as well as dust and some biologically active compounds (at the total concentration 0.125 – 0.25 mg ml^{-1}). The type and amount of admixtures added to the samples were varied according to the law of random numbers. The incubation time was 120 s. Based on the analysis of 65 samples, the assay sensitivity was 1, the specificity was 0.95, the relative risk tended to 0, and the frequency of false positive and false negative results was 1/45 and 0, respectively.

These results and estimates of the DL (see the Table) indicate that the mechanism of HetAI intensification proposed and realized by the author provides a rapid and reliable tool for the detection of single pathogenic organisms in microsamples containing interfering impurities. (An US cell contained 10 and 2 microbial bodies of brucellosis and tularemia bacteria, respectively).

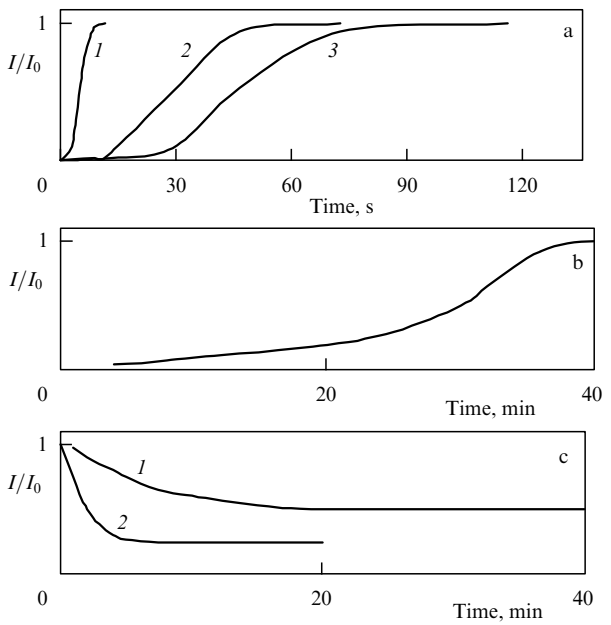

Figure 2. Plots of the luminescence intensity versus the incubation time (a), (b) and wash-out time (c). Figure 2a shows reactions of antigens in an USSW: curve *1* — immunoglobulins ($D \sim 0.04$ μm), curve *2* — chlamydine ($D \sim 0.3$ μm), curve *3* — brucellas (0.4×1.2 μm); Fig. 2b — traditional method (brucella antigen); Fig. 2c: curve *1* — traditional wash-out procedure, curve *2* — washing out in an USSW.

Table. Evaluation of express assay sensitivity.

Immunoactive subject	Sensitivity, microbial bodies per 1 cm^2 (dilution)	
	Instrument	Reference method
Tularemia bacteria	1×10^2	1×10^4
Tetanus toxoid anatoxin	(1 : 1000)	(1 : 200)
Brucellas	5×10^2	1×10^4
Smallpox vaccine virus	(1 : 200)	(1 : 1)
Rickettsia D. *sibiricus*	(1 : 2000)	(1 : 250)

The novelty of the proposed method is protected by the inventor's certificates [10, 11] and the experimental data are published in part in Ref [12].

The validity of the USSW application concept developed by the author and the related technical decisions was confirmed by other researchers who proposed a similar variant of the construction of one- and two-wave chambers for the examination of particle aggregation and acoustic flows in USSW [13], used the Rayleigh acoustic flow and flow US-chambers for the acceleration of mass transfer toward live indicator cells in order to evaluate aquatic toxicity [14], and applied the USSW technique to improve assay sensitivity for the detection of bacterial spores by HetIA in flow chambers [15]. (The last two publications are lacking in the assessment of the applicability of the devices and methods used for the analysis of real samples.)

3. Principles of the construction of highly sensitive optical detectors

Classical photometry of thin-layer objects (IS monolayers in one- or two-wave US cuvettes and optical sensors based on selective plasticized membranes) in transmitted light is associated with impaired sensitivity of the analysis [16]. At the same time, it is known [17] that diffuse radiation is absorbed more effectively than directed radiation, while multiple reflections of the light flux automatically lead to the lengthening of the optical path. It may therefore be expected that mounting thin optically transparent sensitive elements (SEs) on a diffusely reflective substrate and measurements in the transmitted light would substantially improve the assay sensitivity. Adequate theoretical models lacking [18 – 20], we think it appropriate to describe light propagation processes in SEs of a restricted size that are optically conjugated with the reflective substrate.

The sensitive element is a cylinder of diameter D and height l made from an optically transparent material (Fig. 3) and characterized by the dimensionless parameter $g = D/l$, the refraction index n, and the coefficient of extinction ε. The substrate has the reflection coefficient $\rho_b(\Theta')$ and the refraction index n_b.

It is assumed that (a) the light-absorbing components are uniformly spread over the SE volume and the transmission obeys Beer's law, that is, it changes with varying the concentration of the components; (b) the coefficient of light flux reflection near the critical angle Θ_c of the complete inward reflection (CIR) changes jump-wise, and (c) the average height of SE and reflective substrate roughness is much smaller than the probing radiation wavelength.

Let a parallel light flux with the intensity I_0 and transverse cross section $d < D$ be incident perpendicular to the SE surface. (Beams reflected from the substrate are incident on

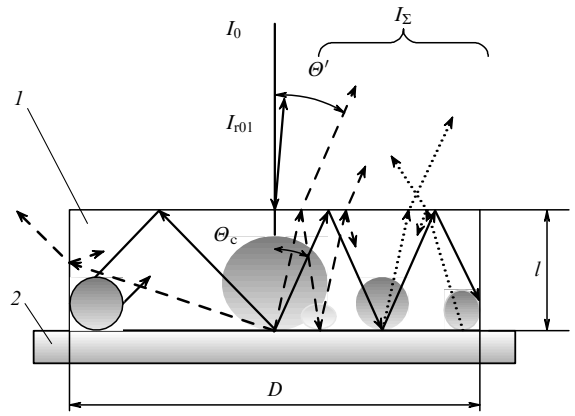

Figure 3. Schematic of light flow distribution in a thin-layer optically transparent element *1* (restricted in size) on a reflecting substrate *2* (see text for details).

the SE – air interface at an angle Θ.) Then, the total intensity of the light flux I_Σ outgoing from SE at an angle Θ' can be written as

$$I_\Sigma = I_0 B(\Theta')[\Phi_1+\Phi_2+\Phi_3+\Phi_4]\,\exp\left[-\varepsilon l\left(1+\frac{1}{\cos\Theta'}\right)\right], \tag{1}$$

where

$$B(\Theta') = \left[1-\rho_{10}(\Theta')\right]\left[1-\rho_{01}\right]\rho_b(\Theta'),$$

$$\Phi_1 = \frac{E(0)\exp(-2\varepsilon l)}{1-E(0)\exp(-2\varepsilon l)},$$

$$\Phi_2 = \int_\delta^{\Theta_1} \frac{\mathrm{d}\Theta}{1-E(\Theta)\exp(-2\varepsilon l/\cos\Theta)},$$

$$\Phi_3 = \rho_c \int_{\Theta_1}^{\Theta_2} \frac{\exp(-2\varepsilon l/\cos\Theta)\,\mathrm{d}\Theta}{1-E(\Theta)\exp(-2\varepsilon l/\cos\Theta)},$$

$$\Phi_4 = \rho_c \int_{\Theta_2}^{\Theta_3} \frac{\rho_b(\Theta)\,\rho_{10}(\pi/2-\Theta)\exp(-2\varepsilon l/\cos\Theta)\,\mathrm{d}\Theta}{1-E\Theta\exp(-2\varepsilon l/\cos\Theta)},$$

$$E(\Theta) = \rho_{10}\rho_b(\Theta), \quad \delta\to 0, \quad \Theta_1 \leqslant \Theta_c = \arcsin\left(\frac{1}{n}\right),$$

$$\Theta_c > \arctan\left(\frac{g}{2}\right), \quad \Theta_2 = \arctan\frac{g-2\tan\Theta'}{4},$$

$\Theta_3 = \arctan(3g/2)$, ρ_{10} and ρ_{01} are the respective reflection coefficients from the SE – air and air – SE interfaces, ρ_c is the critical reflection coefficient, and $\rho_b(\Theta)$ is the substrate reflectance function at the light beam propagation angle Θ in the SE.

Each term in the sum Φ_i in Eqn (1) describes the contribution of different constituents of the flux, viz. Φ_1 is the contribution from multiple reflections of the beam incident normal to the element surface, Φ_2 is the contribution of the first reflection from the substrate in the angle interval $[\delta, \Theta_1]$ and of multiple reflections of the light flux from the butt-end surfaces of the SE, Φ_3 is the contribution of the first reflections from the substrate in the angle range $[\Theta_1, \Theta_2]$ that undergo CIR from the upper ES surface and form light fluxes whose high brightness is comparable to the first reflection, and Φ_4 is the contribution of reflections from the side surfaces of the SE.

Evaluation of the relative contributions of different flux constituents indicates that Φ_1 is smaller than Φ_2 and Φ_3. The magnitude of Φ_2 depends on the reflective properties of the substrate (the contribution of multiple reflections from the side surfaces being small). The contribution Φ_3 is comparable to Φ_2, and the upper boundary of the angle interval is determined by g. The contribution Φ_4 is smaller than Φ_1, Φ_2, and Φ_3 because the coefficients $\rho_b(\Theta)$ and $\rho_{10}(\pi/2-\Theta)$ are much smaller than 1; the angle interval $[\Theta_2, \Theta_3]$ being considered is also small and is close to $\pi/2$.

The largest contribution to I_Σ is made by the first reflection from the substrate and multiple (very bright) reflections depending on CIR conditions. For $g > 10$, the magnitude of I_Σ largely depends on the sums Φ_2 and Φ_3 making the greatest contribution to the resultant light field.

The dependence of the reflection coefficient $r(\Theta')$ on εl can be represented as

$$r(\Theta') = \frac{I_\Sigma}{I_{\Sigma 0}} = \frac{L}{L_0}\exp\left[-\varepsilon l\left(1+\frac{1}{\cos\Theta'}\right)\right], \tag{2}$$

where $I_{\Sigma 0}$ is the background signal (in the absence of photoabsorbing components) and Θ' is the light flux propagation angle outside the SE,

$$L = \sum_1^4 \Phi_i; \quad L_0 = \frac{E(0)}{1-E(0)} + \int_\delta^{\Theta_1} \frac{\mathrm{d}\Theta}{1-E(\Theta)} + \rho_c\left[\int_{\Theta_1}^{\Theta_2} \frac{\mathrm{d}\Theta}{1-E(\Theta)} + \int_{\Theta_2}^{\Theta_3} \frac{\rho_b(\Theta)\,\rho_{10}(\Theta')\,\mathrm{d}\Theta}{1-E(\Theta)}\right].$$

The calculations indicate (Fig. 4a) that even in the case of a poorly reflecting substrate ($\rho_{b0} = 0.1$) in the range $\varepsilon l \in (0; 0.1)$, absorption in the reflected light ($\ln r$) is much higher than in the transmitted light ($\ln t$) and depends on g. For example, the relative amplification of the informative signal $K = ln/ln$ at $el = 0.05$ must be $K = 2.5$ ($g = 2$), $K = 3.6$ ($g = 5$), and $K = 5.1$ ($g = 20$). At $\varepsilon l = 1.0$, $K = 2.4$ ($g = 2$) and $K = 3.1$ ($g = 20$).

The strength of the informative signal registered by a photoreceiver depends on the angle Θ' at which the reflected light flux is recorded and on the angle of the detector field of vision, which, similarly to g, must be chosen as required by the range and sensitivity of measurements.

Experimental verification of theoretical estimates (2) (Fig. 4b) was performed using sensor imitators in the form of HC6, HC7, HC8, HC9, and HC10 neutral glasses ($D = 6$ mm, $l = 0.3$ mm, $g = 20$) placed on a ftoroplast substrate. In the range $\varepsilon l \in (0; 0.1)$, we have $K = 5$, in agreement with the calculated values. In the range $\varepsilon l = 0.12-1.25$, the discrepancy between experimental findings and theoretical estimates did not exceed $\pm 5\%$. The reader is referred to Refs [23, 24] for a detailed discussion of theoretical and experimental data.

To conclude, it has been shown that measurements in reflected light lead to 'autoadjustment' of the optical path length. In other words, the smaller the concentration of the absorbing substance, the longer the optical path of the probing radiation, and vice versa (increased concentration is associated with a decrease in the optical path length). This finding provides a basis for the improvement of sensitivity of measurements at low concentrations and the extension of their dynamical range, i.e., for the creation of conditions allowing the use of a variety of methods to record the

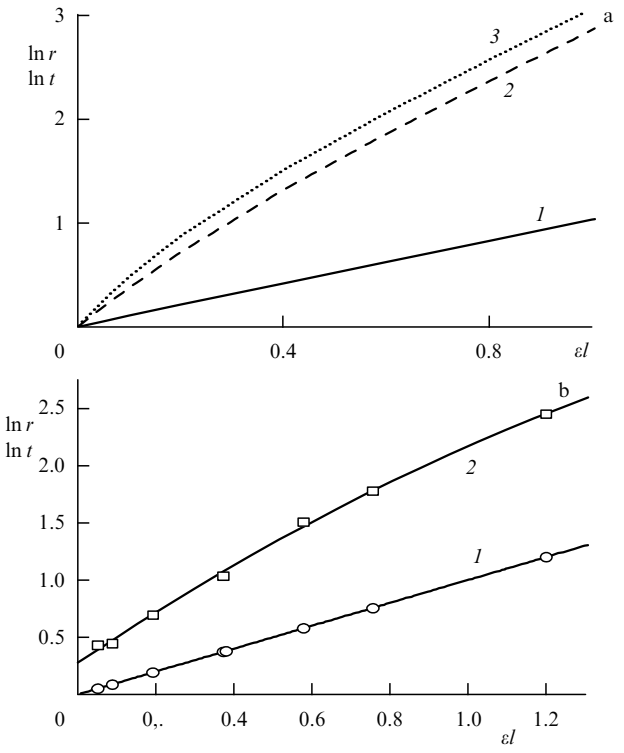

Figure 4. (a) Theoretical dependences of estimated logarithms of the transmission coefficient $\ln t$ (curve *1*) and reflection coefficient $\ln r$ on the value of εl for an SE ($n = 1.45$). Reflectance was estimated for the SE on a diffusely reflective substrate with $\rho_{b0} = 0.1$ at $g = 5$ (curve *2*) and $g = 20$ (curve *3*). (b) Experimental verification of the same dependences for a sensor simulator in transmitted (1) and reflected (2) light at $\lambda = 550$ nm and the reflected light angle 45°.

informative signal (not only by the end-point method but also using the kinetic approach [25, 26]). Kinetic measurements in transmitted light were carried out for the design of fast-acting sensors with the use of selective optically transparent plasticized membranes [25].

4. Study of properties and software–hardware realization of the recurrent algorithm for the evaluation of 'linear trend' signals

The available methods and tools allow analyzing samples using two signal recording modes, i.e., the end-point detection technique and the kinetic regime. In either case, the output signal of the detector has a determinate form with unknown informative parameters to be found. Conversion of the 'signal q–time t' coordinates by introducing a special time scale $\varphi(t)$ and transformation $x(q)$ gives the dependence in the form

$$x = a_0 + b_0\varphi(t) + \xi(t)\,, \tag{3}$$

where a_0 and b_0 are the sought informative parameters and $\xi(t)$ is the additive random noise with an a priori unknown distribution law.

The principal tasks include (a) analysis of the constituent signals of the 'linear trend' type (3); (b) the choice and investigation of algorithms for the evaluation of a_0 and b_0; (c) optimization of algorithms in accordance with the criteria for the minimization of errors and/or the use of computer resources; and (d) software–hardware realization. A series of our publications [27–29] were devoted to solving these problems.

In the majority of cases, the informative parameter is b_0. Passing to the first difference in the summation of trends (3) gives a totality of constant signals with an additive symmetric (hence, centered) noise. The latter problem is effectively resolved with the help of the Fabian–Tsypkin algorithm [30]:

$$c_{n+1} = c_n - \frac{\beta}{n}\,\Psi(c_n - x_{n+1})\,, \tag{4}$$

where

$$\Psi(z) = \begin{cases} -1, & z \leqslant -\Delta \\ 0, & |z| < \Delta \\ 1, & z \geqslant \Delta \end{cases},$$

$x_{n+1} = c^* + \xi_{n+1}$ is the measurement, ξ_{n+1} is the noise, c_n and c_{n+1} are values at the nth and $(n+1)$th estimation steps, β is the algorithm parameter, and 2Δ is the insensitivity zone size (in the case where $\Delta = 0$, $\Psi(z) = \mathrm{sign}(z)$). It is known [30, 31] that estimates ensuing from recurrent algorithm (4) are robust (resistant to bursts), unlike those obtained by the least-square method. The estimation efficiency is generally strongly dependent on the parameters (β, Δ) [31], whose choice is optimized by the criterion of a minimum of estimation error dispersion.

The formerly unexplored case of triangular-shaped (Simpson) noise as the first difference of uniformly distributed noises is described in [27]. It was demonstrated for the first time that only in this case, at the optimal β, Δ ratio, is the estimation error dispersion unrelated to the size of the insensitivity zone.

One of the basic results is the author's original interpretation of algorithm (4) as an automatic control system (ACS) [29] (Fig. 5), which allows the methods of ACSs to be used for the evaluation of its stability, that is, convergence between the estimated c_n and the true c^* values.

An ACS has the following main characteristics: (a) it is discrete, (b) it has two feedback contours, one of them being a negative feedback contour, (c) it contains a nonlinear element K_1 that realizes the function Ψ (a nonideal relay with the insensitivity zone 2Δ); (d) it contains a link with variable parameters $K_2[n]$ that realizes multiplication by β/n; and (e) it has a delay line with a one-step delay and the transfer characteristic K_3.

The conclusion obtained at in Ref. [29] that a given ACS is asymptotically stable in the presence of any zero insensitivity zone has been fully confirmed by other authors.

The following problems were resolved for the practical realization of algorithm (4) in the form of a computing device: (a) the choice of the parameters β and Δ based on extreme

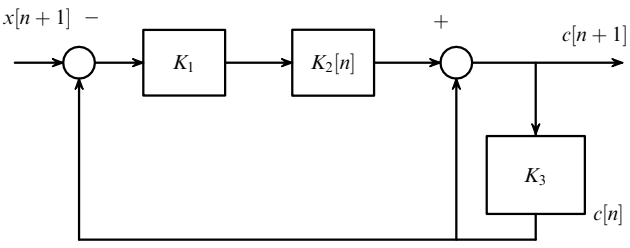

Figure 5. Schematic of an ACS realizing algorithm (3) (see text for the description).

order statistics requiring only a recurrent recalculation of the maximum and minimum elements; (b) the choice of the initial approximation of the estimate as the amplitude center (on the same basis); (c) substantiation of the criterion for the interruption of estimation (needed, for example, because of signal discordance, i.e., a change in the signal trend shape). In addition, we fixed the signs of the nonlinear term in Eqn (4) and constructed and assessed the asymmetry of their histogram [28, 29]. In other words, economical procedures were employed that required no ordering (the search for the median, bend center, etc.).

The device being considered realizes economical computation procedures by virtue of the effective estimation under conditions of the minimal a priori information about random noise parameters. This, in turn, allows realizing the possibility to develop and design a unified computation algorithm and a device compatible with a large variety of instruments for express analyses, including portable and subminiature ones.

5. Conclusion

The prediction and realization of new mechanisms underlying acceleration of immune reactions in HetIA opened up formerly unknown possibilities for the practical utilization of USSW fields

• to develop highly informative methods for the investigation of immunoactive phenomena at the molecular, supramolecular, and cellular levels and

• to construct highly selective devices for sample preparation.

We are currently developing instruments and methods to prepare samples for the identification and characterization of biological subjects based on the analysis of nucleic acid molecules (polymerase chain reaction, in particular, on a real-time scale). In these instruments, the isolation of biological subjects on immunosorbents placed in an USSW field prevents inhibition of the polymerase chain reaction by impurities. Express analysis of immunoactive phenomena containing no nucleic acids, e.g., toxins, is performed with the help of an immune reaction in the USSW field. The method is based on the results of fundamental research into the properties of US fields and the behavior of biological subjects in USSW fields (see Section 2).

The results of the theoretical analysis of the light flow distribution in a formerly unexplored subject of photometry, a thin optically transparent photoabsorbing element restricted in size, have allowed proposing a simple universal scheme of a detector (Fig. 6) that is easy to convert to a multichannel one, e.g., by using fiber-optic technologies [32]. This scheme has found application in a variety of instruments and devices constructed at the Institute of Analytical Instrumentation, Russian Academy of Sciences, that are now available commercially. These are the Imatest-01 analyzer of immunoactive subjects [33]; Nanofor-01 and Nanofor-02 analytical systems for high-performance capillary electrophoresis with spectrophotometric and fluorescent detectors; ANK-16, ANK-32, and ANK-96 nucleic acid analyzers; nucleic acid sequencer (ANPK); laser immunoluminescent cell analyzer; and the Sen and μSen chemosensor analyzers.

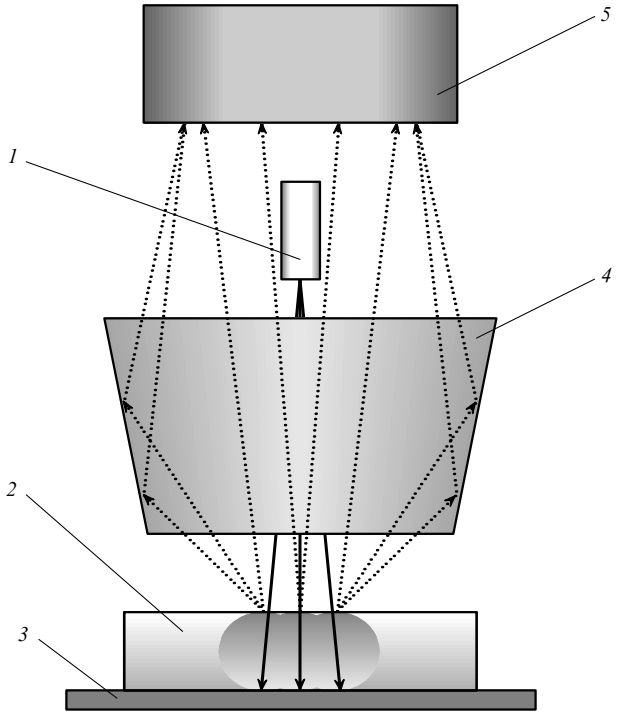

Figure 6. Optical scheme of a reflected light photometer: *1* — emission source, *2* — sensitive element (chemosensor), *3* — reflective substrate, *4* — radiation collector (elliptical mirror), *5* — photoreceiver.

References

1. Ngo T T, Lenhoff H M (Eds) *Enzyme-mediated Immunoassay* (New York: Plenum Press, 1985) [Translated into Russian (Moscow: Mir, 1988)]
2. Egorov A M et al. *Teoriya i Praktika Immunofermentnogo Analiza* (Theory and Practice of Enzyme-Mediated Immonoassay) (Moscow: Vysshaya Shkola, 1991)
3. Widder K J et al. *Clin. Immunol. Immunopathol.* **14** 395 (1979)
4. King L V *Proc. R. Soc. London Ser. A* **147** 212 (1934)
5. Yosioka K, Kawasima Y *Acustica* **5** (3) 167 (1955)
6. Gor'kov L P *Dokl. Akad. Nauk SSSR* **140** (1) 88 (1961) [*Sov. Phys. Dokl.* **6** 773 (1962)]
7. Knyaz'kov N N, Ph. D. Thesis of Technical Sciences (Pushchino: Institute of Biological Physics of the Academy of Sciences of USSR, 1983)
8. Zarembo L K, Krasil'nikov V A *Vvedenie v Nelineinuyu Akustiku* (Introduction to Non-Linear Acoustics) (Moscow: Nauka, 1966)
9. *Metodicheskie Rekomendatsii po Polucheniyu i Primeneniyu Immunoglobulinovogo Sefaroznogo Diagnostikuma dlya Indikatsii Vozbuditelya Ornitoza* (*Psittakoza*) *i Dvukh Vidov Khlamidiyi* (Guidelines on the Preparation and Application of Sepharose Iimmunoglobulin Diagnosticum for the Identification of the Pathogen of Ornithosis (Psittacosis) and Two Chlamydia Species) (Moscow: Minzdrav SSSR, 1981) p. 15
10. Blokhin K V et al. "Sposob postanovki serologicheskoi reaktsii" ("Method of realization of serological reaction"), USSR Inventor's Certificate 1208916, priority of 30.11.83 (1985)
11. Knyaz'kov N N, Kurochkin V E "Sposob vyyavleniya immunoaktivnykh ob'ektov" ("Method for the identification of immunoactive objects"), USSR Inventor's Certificate 1250576, priority of 13.01.84 (1986)
12. Knyaz'kov N N, Kurochkin V E *Byull. Eksp. Biol. Med.* (5) 586 (1996)
13. Spengler J F et al. *Bioseparation* **9** 329 (2000)
14. Morgan J et al. *Toxicology in Vitro* **18** 115 (2004)
15. Hawkes J J et al. *Biosensors Bioelectron.* **19** 1021 (2004)
16. Evstrapov A A, Kurochkin V E, Makarova E D *Nauchn. Priborostroenie* **1** (4) 22 (1991)
17. Gershun A A *Izbrannye Trudy po Fotometrii i Svetotekhnike* (Collected Works on Photometry and Phototechnique) (Moscow: GIFML, 1958)

18. Rozenberg G V *Usp. Fiz. Nauk* **69** (1) 57 (1959) [*Sov. Phys. Usp.* **2** 666 (1959)]
19. Rozenberg G V *Usp. Fiz. Nauk* **91** (4) 569 (1967) [*Sov. Phys. Usp.* **10** 188 (1967)]
20. Zege E P, Ivanov A P, Katsev O L *Perenos Izobrazheniya v Rasseivayushchei Srede* (Image Transfer in a Scattering Medium) (Minsk: Nauka i Tekhnika, 1985) [Translated into English: *Image Transfer Trough a Scattering Medium* (Berlin: Springer-Verlag, 1991)]
21. Ivanov A P *Optika Rasseivayushchikh Sred* (Optics of Scattering Media) (Minsk: Nauka i Tekhnika, 1969)
22. Loiko V A, in *Rasseyanie i Pogloshchenie Sveta v Prirodnykh i Iskusstvennykh Dispersnykh Sredakh* (Light Scattering and Absorption in Natural and Artificial Dispersed Media) (Ed. A P Ivanov) (Minsk: Inst. Fiziki im. B I Stepanova AN BSSR, 1991) p. 355
23. Evstrapov A A, Kurochkin V E *Opt. Zh.* **62** (2) 50 (1995)
24. Evstrapov A A, Kurochkin V E *Opt. Zh.* **62** (5) 40 (1995) [*J. Opt. Technol.* **62** 304 (1995)]
25. Kurochkin V E, Makarova E D *Analytical Commun.* **33** 115 (1996)
26. Burylov D A et al. *Zh. Analit. Khim.* **52** 551 (1997) [*J. Analytical Chem.* **52** 492 (1997)]
27. Bulyanitsa A L, Kurochkin V E *Avtomatika Telemekh.* (9) 187 (1999) [*Automat. Remote Control.* **60** 1368 (1999)]
28. Bulyanitsa A L, Kurochkin V E, Burylov D A *Radiotekh. Elektron.* **47** 343 (2002) [*J. Commun. Technol. Electron.* **47** 307 (2002)]
29. Bulyanitsa A L, Kurochkin V E *Nauchn. Priborostroenie* **12** (2) 30 (2002)
30. Tsypkin Ya Z, Polyak B T *Dinamika Sistem* (12) 22 (1977)
31. Bedel'baeva A A *Avtomatika Telemekh.* (1) 87 1978
32. Kurochkin V E, Evstrapov A A, Makarova E F "Opticheskoe ustroistvo dlya khimicheskogo analiza" ("Optical device for chemical analysis"), RF Patent 2157987, priority of 21.05.1996 (2000)
33. Fedorov A A et al. *Dokl. Ross. Akad. Nauk* **405** (1) 133 (2005) [*Dokl. Biochem. Biophys.* **405** 388 (2005)]

PACS numbers: 42.68.Wt, 95.55.Cs, 95.75.Qr

DOI: 10.1070/PU2006v049n09ABEH006106

Adaptive optical imaging in the atmosphere

V P Lukin

1. Introduction

As is well known, adaptive optics (AO) enjoys effective use in the formation of optical beams and images with the aim of concentrating laser beam energy, improving the sharpness of optical images, increasing the data transfer rate in optical communication lines, and solving other specific problems.

Investigations to develop methods and systems of adaptive optics are being pursued at the Laboratory of Coherent and Adaptive Optics of the Institute of Atmospheric Optics, Siberian Division of the Russian Academy of Sciences. This research is aimed at both elaborating the theory of adaptive systems and developing new elements, models of the systems, and their algorithms.

2. Problems in 'viewing' through the atmosphere

The bulk of information in astronomy is obtained by ground-based instruments. However, inhomogeneities of Earth's atmosphere (refraction, turbulence, radiation-absorbing gases, aerosols) seriously limit the capabilities of astronomical systems. In their papers in the late 1960s, Kolchinskii, Tatarski, and Frid formulated the atmosphere-imposed limitations on astronomical systems. Their results were obtained assuming the Kolmogorov–Obukhov model for the fluctuation spectrum of the refractive index:

$$\Phi_n(\varkappa, h) = 0.033 C_n^2(h)\,\varkappa^{-11/3}\,, \quad \frac{1}{L_0} \ll \varkappa \ll \frac{1}{l_0}\,.$$

Here, $C_n^2(h)$ is the structure parameter of the atmospheric refractive index, h is the current height above the underlying surface in the atmosphere, $\varkappa$ is the wavenumber for turbulent inhomogeneities, and L_0 and l_0 are the inner and outer turbulence scales.

Solving the problem of the optical wave propagation through randomly inhomogeneous media has shown that the phase structure function at a distance ρ obeys the five-thirds power law:

$$D_S(\rho) = 2.91\,k^2 \int_0^\infty \mathrm{d}h\, C_n^2(h)\,\rho^{5/3}\,,$$

where $k = 2\pi/\lambda$ and λ is the radiation wavelength. Proceeding from the last expression, the so-called atmosphere coherence radius r_0 was introduced:

$$D_S(\rho) = 2.91\,k^2 \int_0^\infty \mathrm{d}h\, C_n^2(h)\,\rho^{5/3} = 6.88\left(\frac{\rho}{r_0}\right)^{5/3}\,,$$

which determines the limiting angular resolution $\gamma_0 = \lambda/r_0$ of an optical system in the turbulent atmosphere, the Strehl parameter $\mathrm{St} = \exp(-\sigma^2)$ of the astronomical system atmosphere–telescope (where σ^2 is the variance of phase distortions), the optical transfer function, the point spread function, and other parameters of the astronomical instrument.

Research carried out in the 1960s showed that these theoretical results agree nicely with experimental data obtained for optical apertures of the order of 2–4 m. However, the effective apertures of ground-based astronomical telescopes began to increase swiftly: the 6 m BTA telescope (the Large Azimuth Telescope), the Multiple Mirror Telescope (MMT) with a matrix of six 8 m apertures, the 3.6 m New Technology Telescope (NTT), the 10 m Keck telescope, the 8.2 m Very Large Telescope Interferometer (VLTI), and the 8 m Subaru telescope made their appearance. In this connection, interest was aroused in the study of the phase fluctuations of optical waves in wide-aperture reception.

2.1 Phase fluctuations of optical waves in a turbulent atmosphere

The 1970s saw the development [1, 2] of interference wave phase meters in the optical range for the investigation of turbulent phase fluctuations of the optical wave for long spatial and temporal delays. The phase structure function was found to be sensitive both to the turbulence intensity and to the outer turbulence scale. This compelled reconsidering Tatarski's and Frid's results. In the early 1970s, measurements were made of optical wave phase fluctuations in the USSR (V Pokasov, V Lukin), Italy (L Ronchi, A Consortini), and the USA (G Ochs, S Clifford), with the result that the effect of 'phase structure function saturation' was discovered almost simultaneously [1, 2]. In Refs [1, 3, 4], this effect was interpreted and invoked to describe the spectrum of turbulence with a finite outer scale. We recall that the outer turbulence scale in the Kolmogorov–Obukhov model is assumed to be infinite.

In the 1970s and the 1980s, a consistent theory [1, 2] of phase fluctuations for optical waves propagating through a

turbulent atmosphere was elaborated with the use of turbulence spectra with a finite outer scale:

$$\Phi_n(\varkappa, h) = 0.033 C_n^2(h)(\varkappa^2 + \varkappa_0^2)^{-11/6}, \quad \varkappa_0 = \frac{2\pi}{L_0},$$

$$\Phi_n(\varkappa, h) = 0.033 C_n^2(h)\,\varkappa^{-11/3}\left[1 - \exp\left(-\frac{\varkappa^2}{\varkappa_0^2}\right)\right].$$

Calculations were made of the statistical characteristics of phase fluctuations (variance, correlation functions, spectra, structural function) as the principal distorting factor for imaging systems. It turned out that the variance of image tremor is described [2] by the formula

$$\sigma^2 \approx \int_0^\infty \mathrm{d}h\, C_n^2(h)\left[(2R)^{-1/3} - \left(\frac{1}{4R^2} + \varkappa_0^2\right)^{1/6}\right],$$

where $2R$ is the telescope aperture, whence it is clear that the outer scale begins to exert an effect on the image tremor even when the telescope aperture does not exceed 0.01 of the value of the outer turbulence scale.

As a result, the integral characteristics of astronomical instruments were shown to greatly depend on the astroclimatic characteristics of the atmosphere, among which is the outer turbulence scale. More recently, by using the measurement data of optical wave fluctuations for atmospheric propagation paths, it has been possible to reconstruct the outer turbulence scale and relate its magnitude to the level of thermodynamic atmospheric stability [2].

2.2 Astroclimatic measurements

Our calculations and our theory enabled developing new atmospheric turbulence meters. Several phase fluctuation meters were made for the optical region, in particular, IFAS (analog tracking phase meter), which was tested in 1970–1976, IFUP (angle-of-arrival fluctuations meter), which passed tests on the BTA [2, 3] in 1979–1983, and DIT (differential turbulence meter), which passed tests on the Big Solar Vacuum Telescope (BSVT) in 1996–1999. These systems operated with both laser radiation and the emission of bright (+4) stars (Fig. 1).

The experimental data obtainable with the aid of these devices enable estimating both the atmospheric coherence radius r_0 and the outer turbulence scale L_0. This permitted more accurately determining the atmospheric astroclimate parameters in several regions of Russia: in the Northern Caucasia (Special Astrophysical Observatory), near Lake Baikal (Baikal Astrophysical Observatory), and in the south of the Irkutsk District (Mondy Observatory).

2.3 Effective external scale

In 1997, based on the analysis of astroclimatic measurement data, we introduced the notion of the 'effective outer turbulence scale' [4] for the atmosphere as a whole. The effective outer turbulence scale is introduced as an approximation of the value of the phase structure function $D_S(\rho, C_n^2(h), L_0(h))$, which is calculated using models or the data of direct measurements of the vertical evolution of the turbulence level $C_n^2(h)$ and the outer scale $L_0(h)$. The approximation amounts to setting

$$D_S\big(\rho, C_n^2(h), L_0(h)\big) = D_S\big(\rho, C_n^2(h), L_0^{\mathrm{eff}}\big),$$

i.e., to a different calculation of the structure function: the profile $C_n^2(h)$ is specified according to the model of vertical evolution and the outer scale is assumed to be constant, $L_0(h) = L_0^{\mathrm{eff}}$. This permitted zoning all observatories in the world by the magnitude of the parameter L_0^{eff}. Part of the data are collected in Table 1. At present, this atmospheric parameter, which is a real characteristic of the site of an astronomical instrument, is commonly used. For the world's best observatories, L_0^{eff} ranges between 10 and 30 m [4].

2.4 Development of the theory of anisotropic turbulence

The characteristics of atmospheric turbulence in a surface layer with a plane underlying the surface is adequately

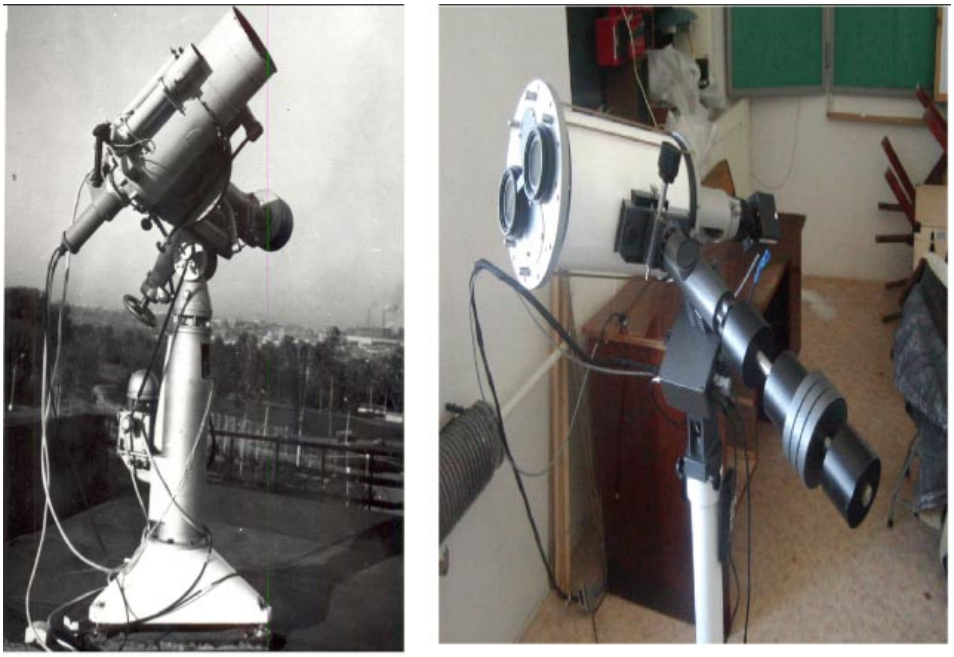

Figure 1. Photometric image tremor measuring instruments for astronomical phenomena: IFUP (a) and DIT (b).

Table 1. Comparison of the measurement data for the external turbulence scale.

Year	Author	External scale, m	Measuring instrument	Measurement site
1983	V P Lukin et al.	8 – 15	Telescope with a 60 cm aperture	Special Astrophysical Observatory (SAO), Russia
1984	Marriotti et al.	8	I2T interferometer	Geodynamical and Astronomical Research Center (CERGA), France
1987	Colavita et al.	> 200	'Mark III' stellar interferometer	Mount Wilson Observatory, USA
1989	Tallon	5 – 8	Hartmann – Shack wavefront monitor	Mauna Kea Observatory, USA
1991	Rigaut et al.	50	'Come-on' adaptive system	La Silla Observatory, Chile
1991	Nightingale	2	Differential image tremor monitor DIMM	La Palma Observatory, Spain
1993	Ziad et al.	5 – 100	Hartmann – Shack wavefront monitor	Haut-Provence Observatory, France
1994	Agabi et al.	50 – 300	GSM1 image tremor meter	Cote d'Azur Observatory, France
1995	Busher et al.	10 – 100	'Mark III' stellar interferometer	Mount Wilson Observatory, USA
1995	Fuchs	1.5 – 2.4	Pilot-balloon-assisted measurements	European Southern Observatory, Cerro Paranal, Chile

described by the Monin – Obukhov similarity theory. In such an isotropic layer, the Monin – Obukhov scale is constant for the whole territory. But above a mountainous relief, stable vortices emerge, and the Monin – Obukhov scale cannot be assumed to be constant in this case. In atmospheric optical research, especially in research into the effect of turbulence on the quality of optical images, we quite often have to deal with an anisotropic boundary layer in the mountains. Therefore, the development of a turbulence theory applicable directly to mountainous conditions has been of interest.

By invoking semiempirical hypotheses of the turbulence theory, we established [5] theoretically and experimentally that the Monin – Obukhov similarity theory in an arbitrary anisotropic layer is fulfilled locally, in the neighborhood of each point in the layer. Consequently, an arbitrary anisotropic layer is locally weakly anisotropic. The main parameter of turbulence in such a layer is the variable Monin – Obukhov number.

The theoretical and experimental data for the Tatarski outer scale L_0^{T} in the mountainous boundary layer in the Lake Baikal region are compared in Fig. 2. A comparison of the L_0^{T} scales measured in three different ways (by Tatarskii's definition, from saturation using spectra, and from the 5/3 dependence using spectra) shows that the results of experiments and the semiempirical theory for an anisotropic boundary layer are in satisfactory agreement [5, 6].

3. Development of the theory and practice of atmospheric adaptive systems

In 1977, we began investigating the feasibility of applying phase correction to reduce the atmospheric effect on the parameters of optical systems. The elaboration of the theory of atmospheric adaptive optical systems [2, 6] was substantially completed during the 1984 – 1986 period. The main results were published in the monograph Ref. [2] (1986), which was translated into English and published in the USA in 1996. We emphasize the most significant results.

Reference [6] (1979) for the first time described two-color adaptive systems for which the wavelengths of the main and reference radiation do not coincide.

Using the optical signal scattered from atmospheric irregularities for producing the reference signal was first proposed in Refs [7, 8]. In our first publication devoted to this question, which dates back to 1979, calculations were made of the cross-correlation function for the phase fluctuations of a Gaussian beam and the plane reference wave. Lukin and Emaleev [7] came up with the idea of employing the signal of backscattering from atmospheric irregularities for image correction. Lukin and Matyukhin [8] calculated the max-

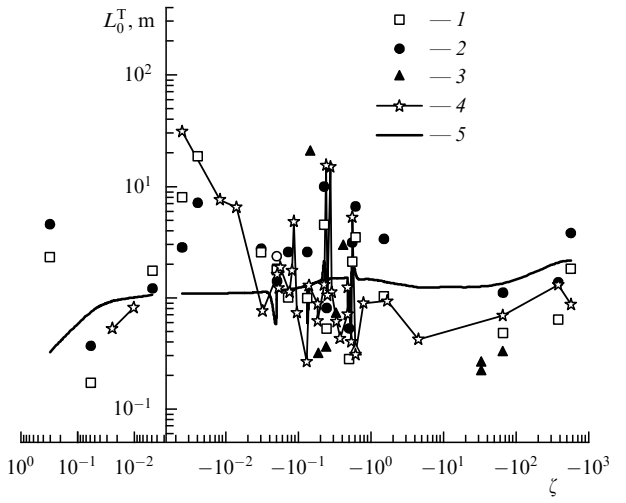

Figure 2. Comparison of experimental and theoretical data for the outer turbulence scale L_0^{T} in a mountainous anisotropic boundary layer; ζ are the dimensionless Monin – Obukhov numbers calculated from the data of weather stations. The experimental data were obtained from the 5/3 power-law dependence using spectra (*1*), from saturation using spectra (*2*), and from Tatarskii's definition (*3*). Curve *4* corresponds to the semiempirical theory for an anisotropic layer and curve *5* to the semiempirical theory for an isotropic layer.

imum image correction attainable in a telescope with the use of a reference source formed at a fixed distance in the atmosphere.

Today, this research has received wide acceptance, and a new scientific area has emerged: the production and application of laser reference stars.

Using statistical fluctuation prediction was first proposed for the study of the dynamic properties of adaptive systems. Zuev and Lukin [9] analyzed the adaptive systems as dynamic systems. Apart from conventional permanent-lag adaptive systems, the capabilities of 'fast' systems as well as of 'predictive' adaptive systems were considered. The longest permissible time delays that ensure the requisite correction level for adaptive systems were determined. It was found that they are defined by the effective wind speed, the atmospheric coherence radius, and the parameters of the optical system.

During the same period, principles were elaborated and prototypes were made [8, 10 – 14] of the individual components of an adaptive optical system: compound multicomponent mirrors, mirrors for the fast control of the wavefront tilt, flexible bimorph optical elements, dissector and coordinate-sensitive photodetector tracking systems. Using the prototypes of the individual components of adaptive systems, experiments were carried out [7] in the phase correction of turbulent and refractive distortions in optical imaging and the formation of laser beams in the atmosphere in 1981.

4. Adaptive optical system for telescopes

In 1993 – 1994, under the task of the Ministry of Science of the Russian Federation, an adaptive optical system was developed for the AST-10 telescope (Russian project of an adaptive compound 10-meter telescope). The telescope itself, which has a compound 91-element mirror, turned out to be too slow for real-time compensation of turbulent distortions. That is why, proceeding from an analysis of world experience in the development of suchlike systems, a correction concept was proposed, which employed an adaptive secondary mirror. The entire optical system of the telescope was modeled, beginning with errors in the alignment of its primary mirror [15 – 18]. A telescope scheme proposed during the execution of the project comprised an adaptive secondary mirror and a mirror controllable in two angles to stabilize the image as a whole.

Also investigated were the feasibility of partial phase correction of the image with the aid of an adaptive secondary mirror, different turbulence levels on the basis of atmospheric models, different types of active mirrors (compound, flexible, and mode mirrors), and different wavefront measuring instruments [15 – 19]. We studied the effect of misphasing the AST-10 primary mirror by the magnitude of the Strehl parameter.

The telescope's point spread function was calculated for a partial correction of turbulent distortions. Both compound and flexible mirrors with a different number of constituent elements were considered. Also investigated was the effect of the fluctuation of the number of photons in the incoming light flux during adaptive system operation with the radiation of faint stars. The operational capabilities of the telescope were calculated in the case where a laser reference star is used [18 – 20].

A study was made of the effect of a turbulent atmosphere on the signal in long-base interferometers, including stellar interferometers. The phase difference spectra were calculated analytically and numerically for the signals in stellar interferometers with different bases for different orientations of the wind velocity vector and the interferometer base, different turbulence spectra and wind speed models being used in this case [18]. Figure 3 shows the spectra of the phase difference in stellar interferometers with different bases: 3, 12, 38, and 85 m. The solid and dashed curves correspond to the longitudinal and perpendicular mutual orientations of the interferometer base and the wind velocity. Therefore, choosing the adequate

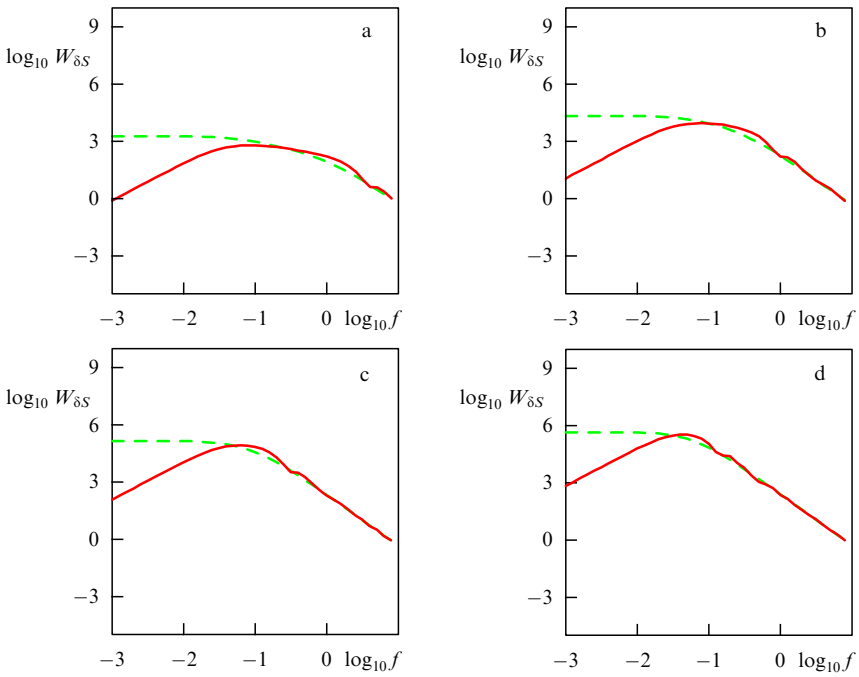

Figure 3. Frequency spectra $W_{\delta S}(f)$ of phase difference fluctuations δS for interferometers with different bases: (a) 3 m, (b) 12 m, (c) 38 m, (d) 85 m; δS is a dimensionless quantity, the frequency f is measured in Hertz.

model for the altitude curve of the outer turbulence scale has been shown to be of paramount importance.

5. Adaptive solar telescope

We made an attempt to apply an AO system to the BSVT of the Institute of Solar–Terrestrial Physics, Siberian Division of the Russian Academy of Sciences. The first season was devoted to the collection of data on the daytime astroclimate of the Lake Baikal region. The DIT (differential image tremor) monitor of our design was used (see Fig. 1). The behavior of solar image distortions arising from the characteristic properties of this region was investigated. On this basis, the first-version AO system for the BSVT was developed [20]. Its task is to afford the operation of the system when a contrast 'spot' or a 'pore' is within the field of view of the wavefront monitor (Fig. 4a).

The prototype of the AO system, which comprised a device for measuring the displacement of the image center-of-gravity, stabilized a fragment of the solar image. A spot (a pore) on the solar surface was selected as the element for tracking. The image quality was improved by a factor of 4–16. Use was made of a two-coordinate-controllable mirror (Fig. 4b) with a piezoceramic drive (two such mirrors were delivered to the Nanjing Astronomical Instruments Research Center in China).

The adaptive system test data showed that the system was highly efficient during operation with a contrasting subject. Further progress in this direction involves the development of the prototype of an image displacement monitor with a capacity for work in conditions of small intensity variations. During the test operation of the adaptive optical system at the BSVT in 2004 and 2005, the contrast of the granulation pattern in different regions of the solar disk ranged between 1% and 4% on average (Fig. 5). In operations with a low-contrast image, a correlation algorithm for measuring image fragment displacements was used. The latest version of our adaptive system is employed to measure the image displacement of the solar granulation pattern on the basis of a modified correlation tracking algorithm [22]. Figure 6 displays persistent stabilization of a surface fragment of the solar surface. The image contrast for a 'long' (2 s) exposure in the tracking mode remains almost the same as for a 'short' (2 ms) exposure.

As a development of the above activities, we proposed the 'Angara' adaptive correction system for the correction of higher-order wavefront aberrations, which comprises a flexible multielement mirror and a wavefront monitor.

6. Laser guide stars

Laser guide stars (LGSs) are used in astronomy because the energy of radiation of weak stars is too low to furnish simultaneous operation of adaptive systems and the telescope itself. In work dating back to 1979–1980 [2, 8], it was shown for the first time that the backscattering signal from atmospheric irregularities can be used as a reference beacon. Several scientific experiments were carried out in the Astrofizika Research and Production Association and in our laboratory. Their results were published in the open press in the USSR and abroad. Meanwhile, a start on similar research in the USA was made in approximately 1982, and this research was classified until 1993.

Despite the attractiveness of the LGS technique, it suffers from one major disadvantage: there is practically no way of correcting the general slope of the wavefront. This problem

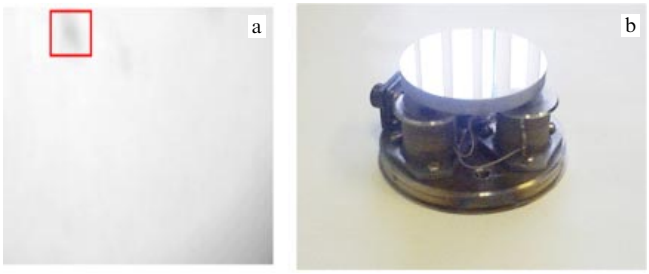

Figure 4. (a) Detail of a solar surface image in the BSVT. (b) Correcting mirror.

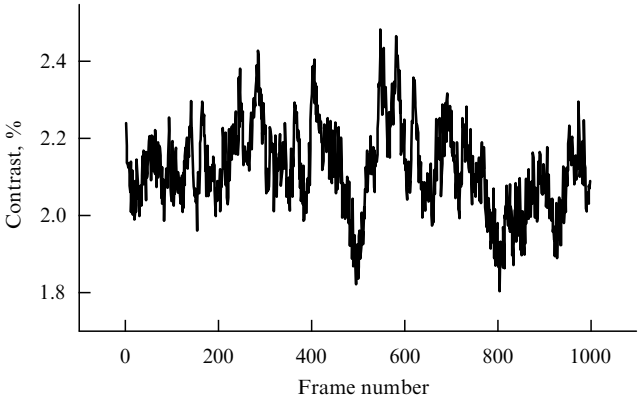

Figure 5. Contrast of a solar granulation image near a spot measured at the primary focus of the telescope. The detector field of view measures 29×29 arc seconds.

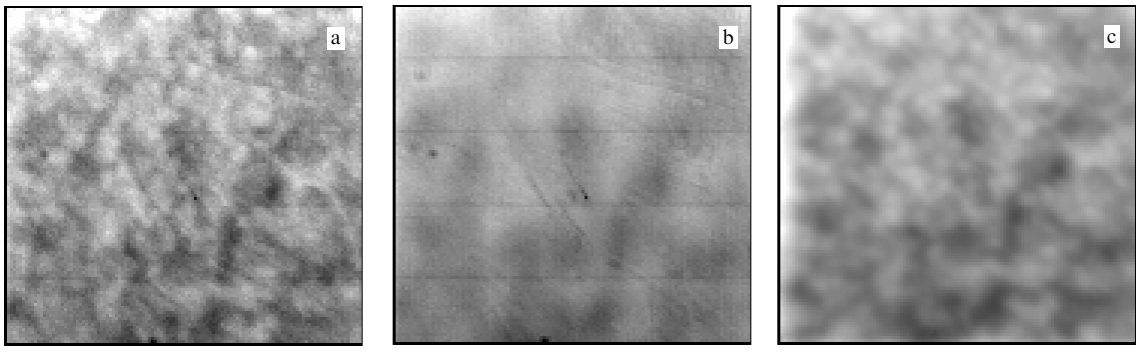

Figure 6. Photographs of the granulation image obtained (a) in the mode of short exposure (2 ms), (b) in the 'long exposure' mode (2 s) without control, and (c) in the 'long exposure' mode (2 s) with a modified correlation monitor.

has been stated in several papers, including our 1996 papers [17 – 19]. One possible way to solve this problem [17, 18, 21 – 23] involves using the optimal correction algorithm, which minimizes the residual distortions of the wavefront tilt arising from fluctuations. The gist of this algorithm consists in scaling the measurement data for the location of an LGS image with the aid of a weighting coefficient obtained either by calculations or by direct measurements.

We have proposed a hybrid scheme, which is free of several drawbacks of the previous analogs, and a new approach to the dynamic formation of LGSs. We have shown that using an LGS in the form of a reference cross produced by scanning two narrow laser beams affords efficient correction of wavefront tilts even for wide-aperture telescopes [21, 22].

7. Phasing of compound mirrors

The use of a large compound primary mirror in a telescope brings the additional problem of phasing the multielement compound mirror with an optical accuracy. We considered the distortions in a ground-based telescope caused by misphasing of the segments of the primary mirror [22 – 24]. The corresponding decrease in the Strehl parameter may be judged by Fig. 7, which allows comparing the data of a numerical experiment with the results of theoretical investigations. One can see that random displacements and tilts of mirror segments result in significant image distortions. In particular, under displacements with a variance of the order of one wavelength, the Strehl parameter decreases by a factor of five or more in comparison with the diffraction-limited value. The correction of random segment shifts with an amplitude of several hundred wavelengths is normally effected with the aid of capacitive or inductive surface sensors. At the same time, it is possible to compensate for displacements on the basis of purely optical techniques. An interference criterion based on a reference interference pattern was used as the goal control function. In the initial stage of investigations, the following optical arrangement was used for this purpose. Special reflective plates were affixed at the interfaces between the segments. The center-of-gravity positions of the beams reflected from each of the plates were recorded in the plane of observation. Their displacements were determined to permit evaluation of random shifts of the segments. The determination of the shifts was followed by their compensation, which was either automatic, for instance with the use of the aperture probing algorithm, or by manual alignment.

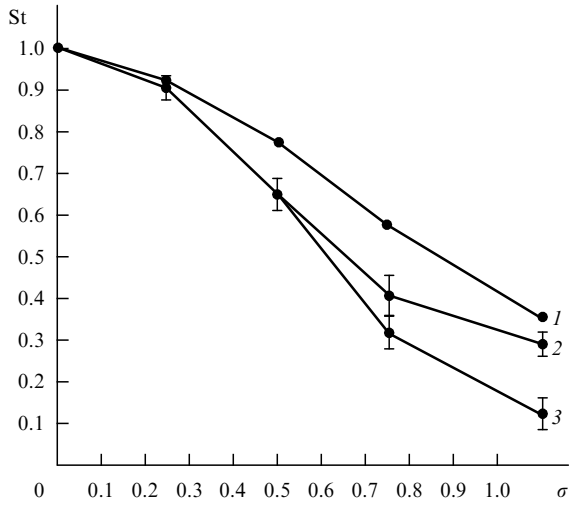

Figure 7. The strehl parameter as a function of the random-shift variance normalized by the radiation wavelength: theoretical results (curve *1*) and data derived from a numerical experiment for a mirror with the number of segments 32×32 (curve *2*) and a mirror with the number of segments 8×8 (curve *3*).

Simple estimates show that a relative segment shift of 10 μm results in a centroid displacement by the distance Δz about 0.1 mm in the plane located at the distance 1 m from the segmented mirror surface. In the calculations, the longitudinal dimension of the plates was assumed to be about 1 cm. The above displacement can be reliably recorded by modern digital video cameras. It may therefore be concluded that the proposed algorithm enables phasing the compound mirror surface with an accuracy of 1 – 2 wavelengths even when the initial relative shift is far greater than the wavelength.

We proposed a phasing algorithm allowing us to decrease the residual shifts of mirror segments to values far less than the optical radiation wavelength. Coherent beams produced by a laser source were reflected from two neighboring elements and directed to a common spot by beam-deflecting mirrors. Recorded in the plane of observation was an interference pattern, in which the fringe positions were determined by the relative phase shift of the beams. To bring the elements into phase, the aperture probing algorithm was used with the beams controlled only in one coordinate.

In this case, the interference criterion constructed with the use of the reference interference pattern was chosen as the goal function. Early in the investigation, the segments were brought into phase at the wavelength $\lambda = 0.8$ μm. Numerical experiments showed that the algorithm under consideration enabled compensating for the segment misphasing when the initial shifts were smaller than the wavelength, $\Delta z = 0.367$ μm. When the shift exceeds half the wavelength, the algorithm diverges, which results in an increase in segment shifts. The admissible range in initial shifts can be broadened by introducing an additional wavelength into the control algorithm. In particular, the values of the criterion calculated for different relative segment shifts for the wavelengths $\lambda = 0.6$ and $\lambda = 0.8$ μm are given in Fig. 8. It can be seen from Fig. 8 that physical segment shifts of the same length give different phase shifts for different wavelengths. The peaks of the criteria coincide only for the shifts $\Delta z = 0$ and $\Delta z = 2.4$ (-2.4) μm. The range of shifts that can be compensated is additionally broadened by selecting the

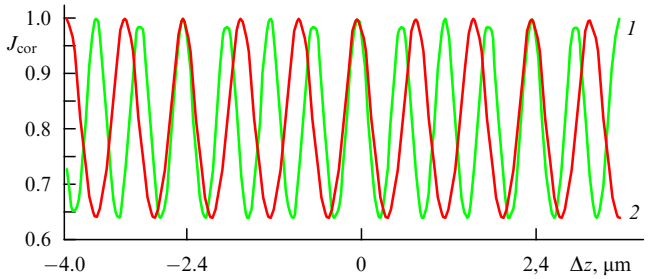

Figure 8. Correlation criterion J_{cor} versus relative shift Δz of mirror segments. Curve *1* corresponds to a wavelength $\lambda_1 = 0.6$ μm and curve *2* to a wavelength $\lambda_2 = 0.8$ μm.

Table 2. Maximum permissible shift Δz whereby the mirror surface can be phased in. λ_i are the wavelengths at which the control is effected.

λ_1, μm	λ_2, μm	λ_3, μm	Δz, μm
0.8	—	—	0.36
0.6	—	—	0.26
0.6	0.8	—	2.34
0.7	0.8	—	5.55
0.6	0.7	0.8	33.4

wavelengths of the interfering beams. Finally, the range may be radically broadened by introducing the third wavelength. Numerical experiments showed that the phasing for $\lambda_1 = 0.6$, $\lambda_2 = 0.7$, and $\lambda_3 = 0.8$ μm is effected for the initial shift $\Delta z = 2.34$ μm. The data characterizing the admissible range of the shifts are collected in Table 2.

In conclusion, we summarize the work of the Institute of Atmospheric Optics, Siberian Division of the Russian Academy of Sciences, on the problem of the application of atmospheric optics for the improvement of viewing through the atmosphere as a randomly inhomogeneous medium. The proposed techniques and the prototypes of the corresponding systems have successfully passed laboratory and full-scale tests to demonstrate that even the application of simple AO systems yields a substantial gain. The systems elaborated at the Institute of Atmospheric Optics can be applied in optical viewing systems and astronomical devices for routine operation.

References

1. Lukin V P, Pokasov V V *Appl. Opt.* **20** 121 (1981)
2. Lukin V P *Atmosfernaya Adaptivnaya Optika* (Atmospheric Adaptive Optics) (Novosibirsk: Nauka, 1986) [Translated into English (Bellingham, Wash.: SPIE Press, 1995)]
3. Gubkin S M et al. *Astron. Zh.* **60** 789 (1983) [*Sov. Astron.* **27** 455 (1983)]
4. Lukin V P *Opt. Atm. Okeana* **10** 516 (1997) [*Atm. Oceanic Opt.* **10** 322 (1997)]
5. Nosov V V et al. *Opt. Atm.* **18** 845 (2005) [*Atm. Oceanic Opt.* **18** 756 (2005)]
6. Lukin V P *Opt. Lett.* **4** 15 (1979)
7. Lukin V P, Emaleev O N *Kvantovaya Elektron.* **7** 1270 (1980) [*Sov. J. Quantum Electron.* **10** 727 (1980)]
8. Lukin V P, Matyukhin V F *Kvantovaya Elektron.* **10** 1264 (1983) [*Sov. J. Quantum Electron.* **13** 814 (1983)]
9. Zuev V E, Lukin V P *Appl. Opt.* **26** 139 (1987)
10. Emaleev O N, Lukin V P *Kvantovaya Elektron.* **9** 2264 (1982) [*Sov. J. Quantum Electron.* **12** 1470 (1982)]
11. Lukin V P et al. *J. Opt. Soc. Am. A* **11** 903 (1994)
12. Lukin V P *Proc. SPIE* **2222** 527 (1994)
13. Vitrichenko E A et al. *Problemy Opticheskogo Kontrolya* (Optical Check Problems) (Executive Ed. I V Samokhvalov) (Novosibirsk: Nauka, 1990)
14. Vitrichenko E A et al. *Dokl. Akad. Nauk SSSR* **300** 312 (1988) [*Sov. Phys. Dokl.* **33** 309 (1988)]
15. Fortes B V, Lukin V P *Proc. SPIE* **1688** 477 (1992)
16. Lukin V P et al. *Proc. SPIE* **2222** 522 (1994); *Opt. Atm. Okeana* **8** 409 (1995) [*Atm. Oceanic Opt.* **8** 210 (1995)]
17. Lukin V P, in *Adaptive Optics. Proc. of a Topical Meeting, October 2–6, 1995, Garching, Germany* (ESO Workshop Proc., No. 54, Ed. M Cullum) (Garching bei München: European Southern Observatory, 1996) p. 373
18. Lukin V P, Fortes B V *Astron. Zh.* **73** 419 (1996) [*Astron. Rep.* **40** 378 (1996)]
19. Lukin V P *Opt. Atm. Okeana* **9** 1433 (1996) [*Atm. Oceanic Opt.* **9** 910 (1996)]
20. Lukin V P et al. *Opt. Atm. Okeana* **12** 1161 (1999) [*Atm. Oceanic Opt.* **12** 1107 (1999)]
21. Lukin V P *Appl. Opt.* **37** 4634 (1998)
22. Lukin V P et al. *Opt. Zh.* **73** (3) 55 (2006) [*J. Opt. Technol.* **73** 197 (2006)]
23. Lukin V P, Fortes B V *Adaptivnoe Formirovanie Puchkov i Izobrazhenii v Atmosfere* (Adaptive Beaming and Imaging in the Turbulent Atmosphere) (Novosibirsk: Izd. SO RAN, 1999) [Translated into English (Bellingham, Wash.: SPIE Press, 2002)]
24. Kanev F Yu, Lukin V P *Adaptivnaya Optika. Chislennye i Eksperimental'nye Issledovaniya* (Adaptive Optics. Numerical and Experimental Research) (Tomsk: Izd. Inst. Optiki Atmosfery SO RAN, 2005)